ΠΟΛΥΤΕΧΝΕΙΟ ΚΡΗΤΗΣ
TECHNICAL UNIVERSITY
OF CRETE

Title: A Low cost EEG SSVEP-based Brain Computer Interface for navigation applications

Author: Nikolaos Zacharioudakis

Head: Prof. Zervakis Michael, Technical University of Crete
Advisor: Prof. Dollas Apostolos, Technical University of Crete
Supervisor: Dr. Sakkalis Evangelos, Research Director, FORTH-ICS

School of Electrical and Computer Engineering
Technical University of Crete

Summary

There has been an increase in the number of studies lately focusing on Brain Computer Interface (BCI) systems and non-invasive scalp Electroencephalography (EEG) measurement, with Steady State Visual Evoked Potential (SSVEP) playing a significant role due to its higher Information Transfer Rate (ITR) and signal-to-noise ratio, as well as its minimal training requirements. The SSVEPs can be acquired in the occipital and parietal lobes, but selecting different EEG channel combinations and adapting data length to each subject's specifics promises better results.

The present study aims to improve further existing systems, relying on SSVEPs, with an equally efficient and accurate one, that is more cost-effective thus offering a solution to a serious problem for those facing mobility disabilities or are quadriplegic and are not visually impaired. Moreover, the possibility of replacing wet electrodes with dry ones is being studied. One of the objectives, therefore, is to offer the opportunity for those with limited or no mobility to become mobile and self-reliant in their daily life. As a proof of principle, a robotic car equipped with a video capturing device was used, with the potential to be replaced by a wheelchair in the future.

In this study, data were collected using two types of electrodes, wet and dry, with the latter being more sensitive to noise. Nonetheless, using dedicated signal processing techniques and more specifically Canonical Correlation Analysis (CCA) one can increase the accuracy for SSVEP detection. Finally, the main target of this study is to design a practical BCI system focusing on low-cost hardware and software, easy to use, and robust with increased performance.

Acknowledgments

Abbreviations

BCI	Brain Computer Interface
EEG	Electroencephalography
EMG	Electromyography
ECG	Electrocardiogram
MEG	Magnetoencephalography
LDA	Linear Discriminant Analysis
CCA	Canonical Correlation Analysis
ICA	Independent Component Analysis
PSD	Power Spectral Density
KNN	K-Nearest Neighbor
SVM	Support Vector Machine
ERP	Event Related Potentials
SCP	Slow Cortical Potential
SMR	Sensorimotor Rhythm
EP	Evoked Potential
ITR	Information Transfer Rate
SSVEP	Steady State Visual Evoked Potential
GUI	Graphical User Interface
AC	Alternating Current
BLE	Bluetooth Low Energy
SoC	System On a Chip
FFT	Fast Fourier Transform
SNR	Signal to Noise Ratio

GDPR   General Data Protection Regulation

fMRI   functional Magnetic Resonance Imaging

FNIRS   Functional Near-Infrared Spectroscopy

Contents

List of Figures

List of Tables

CHAPTER 1

Overview

1.1 Goals and contributions

The existing research [1], this thesis is based on, uses a BCI system based on the SSVEP method. More specifically when the subject focuses its gaze on a light source that is flickering with a steady frequency, the very same frequency can be detected on the EEG signals of the occipital lobe. In that system, four targets/checkerboards reverse their pattern on a computer screen, each one using a different frequency. An EEG recorder captures the user's brain signals constantly. In real-time, when the user focuses on a specific target, the target's frequency can be easily detected in the captured EEG, using specific algorithms Each target is associated with a distinct movement of a robot. Therefore, if, for example, the user focuses its gaze on the upper target, the algorithm will recognize the corresponding frequency and send, wirelessly, the FORWARD command to the robot.

The correspondence of the remaining targets is:

- lower target – MOVE BACKWARDS

- right target – TURN RIGHT

- left target – TURN LEFT

In case no target is recognized -when the user focuses on the center of the screen- the robot stops moving. The software of the system is developed using Python. A Linear Discriminant Analysis (LDA) classifier is trained to recognize each one of the five classes (4 targets + center of the screen → forward, right, backward, left, stop commands) through a short training session. After the training, the user can run the system in real-time in order to navigate the using vehicle. EEG signal recording is performed using a commercial EEG recorder, the g.MOBILab of the g.tec company, which includes eight monopolar wet electrodes, with a gold-plated 10mm diameter cup.

This study focuses on the below modifications:

1. The use of the open-source openBCI board as an EEG recorder. The board should be incorporated in the pre-existing system and run with the python software.

2. The use of the new dry electrodes g.SAHARA in the place of the wet electrodes, typically used. Dry electrodes are very convenient and easy to wear, as they do not require any conductive gel compared to wet, but they present a lower Signal to Noise Ratio (SNR). To fully maximize the SNR, the duration of the training sessions increased, a higher window size was used, and heavier filtering was added to reduce the Alternating Current (AC) frequency during preprocessing.

1.2   Thesis outline

- **Chapter 2 - Introduction**

  This chapter describes the theoretical background needed to understand and accomplish this study. More specifically, it analyzes the brain anatomy and its most significant functions, explains what the electroencephalography is, what the detected brain activity patterns on an EEG are, and how to trace on it the signals not generated by the brain, the called artifacts. In addition, it presents the various types of electrodes and how to place them in the scalp to receive the brain signals properly. Another significant part is the analysis of the BCI and specifically the SSVEP, which this study has used. Finally, it introduces the main algorithms used in data analysis, the CCA and the LDA.

- **Chapter 3 - Related work**

  This chapter presents the research for the existing BCI system this thesis is based on.

- **Chapter 4 - Methodology**

  This chapter describes the experimental procedure. In particular, it refers to the hardware components of the BCI system and the GUI developed for the needs of the study, and it presents the methods used for the data analysis. Additionally, it describes how the offline experiment

is used for the model training. Finally, it explains the real-time trial the subjects underwent in order to evaluate the system's performance.

- **Chapter 5 - Results**

  This chapter introduces the system's performance evaluation under specific metrics through the collected EEG records from training and online session.

- **Chapter 6 - Discussion**

  This chapter comments on the results and compares the system with other high-cost commercially available solutions.

- **Chapter 7 - Conclusion**

  In this chapter, a concluded opinion about the study, suggestions for future improvements, and extensions are provided.

CHAPTER 2

Introduction

2.1 Brain

The brain constitutes the most complex organ of humans that controls thoughts, motor skills, vision, and so many other processes that regulate our body. Despite the evolution of technology over the last three decades, there is still much to be understood of its operating mechanisms and the array of opportunities of combining the brain with a machine.

2.1.1 Physiology
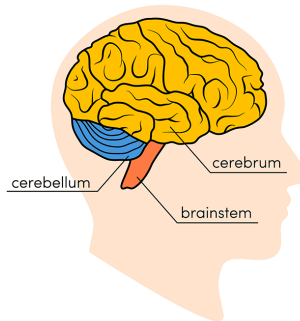
Figure 2.1. Human brain anatomy [2].

The human brain is composed of three main parts, cerebrum, cerebellum, and brainstem, as depicted in figure 2.1 [2–4].

- The cerebrum is the largest part of the brain, it is composed of the right and the left hemispheres, and it is mainly responsible to perform higher functions like vision, hearing, learning, control of movement, and touch.

- The cerebellum is located at the back of the head, under the cerebrum, below the temporal and occipital lobes, and above the brainstem. Its function is to coordinate muscle movements, maintain posture balance and equilibrium.

- The brainstem acts as a relay center connecting the cerebrum and cerebellum to the spinal cord. It performs many automatic functions such as breathing and heart rate.
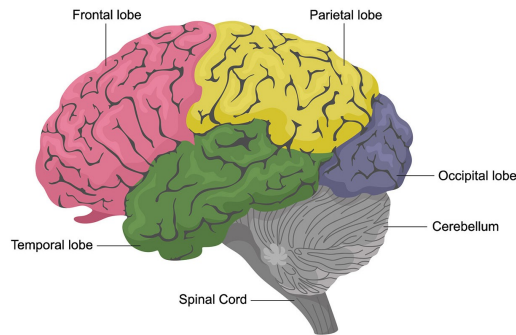
Figure 2.2. Human brain anatomy [2].

Proceeding to a more detailed analysis, as figure 2.2 shows, the cerebral part of the brain consists of two hemispheres, divided into four lobes, frontal, temporal, parietal, and occipital, each one may be divided into other areas that serve specific functions. It must be mentioned that there are complex relationships between the lobes, and none of them can function alone [2–4].

- The **frontal** lobes are the largest ones of the brain, they are located in the front of the head, and they are responsible for personality, judgment, problem-solving, and motor function. Moreover, they contain Broca's area, which is associated with Speech ability.

- The **parietal** lobes are the middle part of the brain and could be described as a sensory strip as they are involved in interpreting pain and touch in the body. Even more, they are responsible for interpreting signals from vision, hearing, and motor and understanding spatial relationships and visual perception. Interpretation of the language and words is another function that must be mentioned.

- The **occipital** lobes are placed in the back part of the brain and contain the brain's visual processing system.

- The **temporal** lobes lie in the side of each hemisphere. In the posterior third of the upper temporal convolution of the left hemisphere is located the Wernicke's area, which in cooperation with the Broca's area, are the language comprehension center. In addition, these lobes are involved in short-term memory, hearing, and smell recognition.

2.2   Electroencephalography

EEG is defined as the electrical activity recorded from the scalp using metal electrodes and conductive medium, according to Michal Teplan [5]. EEG belongs to non-invasive signal acquisition methods along with Magnetoencephalography (MEG), functional Magnetic Resonance Imaging (fMRI), and Functional Near-Infrared Spectroscopy (FNIRS), in other words, brain activity is measured using external sensors without neurosurgically implanted electrodes [6].

An EEG recording may be divided into three main categories, the normal activity, the artifacts, and the evoked potentials [7].

2.2.1   Brain activity patterns

Normal

In EEG, the oscillating electrical voltages in the brain are called brain waves, and they are categorized into five principal bands based on their frequency range, Gamma, Beta, Alpha, Theta, and Delta, as shown in figure 2.3 [9–11].

- **Delta (0.5-4 Hz)** is the lowest frequency and the highest one in amplitude. Normally it is located frontally in adults and posteriorly in children and usually found during sleep or continuous attention tasks. It should be noted that the inappropriate Delta response translates into a lack of focus ability and drastically limit on keeping attention.

- **Theta (4-8 Hz)** is characterized as slow activity and can be observed during internal focus, meditation, spiritual awareness, and on state between wakefulness and sleep. While the existence of this band during wakeness in children up to 13 years old is normal, in awake adults it is
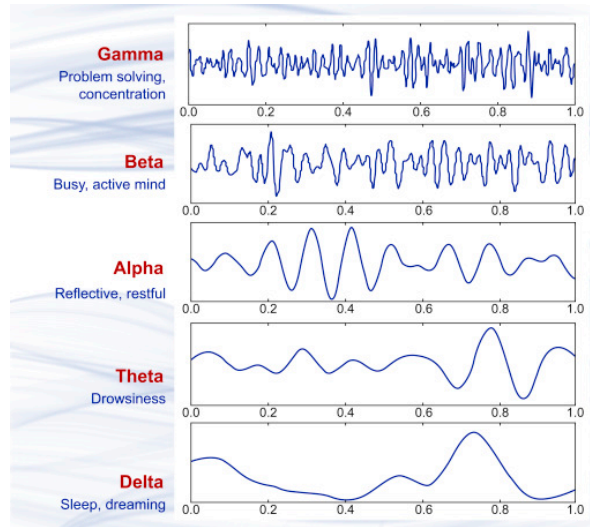
Figure 2.3. Brain wave samples with dominant frequencies belonging to beta, alpha, theta, and delta bands and gamma waves [8].

a signal of abnormality and can be translated as a focal disturbance in focal subcortical lesions.

- **Alpha (8-12 Hz)** band is detected in the occipital lobes with the dominant one featuring the higher amplitude. Its frequency range is 8–12 Hz and has its greatest peak at 10Hz. In addition, it becomes visible in concentration, as well as when the subject is mentally inactive, yet alert, with eyes closed, and it reacts to movements such as eye-opening and sudden alerting.

- **Beta (12-35 Hz)** is normally found in adults with low amplitude while thinking, paying attention, and active concentration. Usually, seen on both sides of the frontal lobe, thus **Beta** rhythm and especially Rolandic, one of the two types of this band, is closely linked to motor behavior. The second and last type of **Beta** band is frontal and it appears during cognitive tasks related with decision-making.

- **Gamma rhythms (>35 Hz)** depict higher mental activities such as fear and perceptions, and it is the only band that can be found in every part of the brain. Moreover, it plays a significant role in finger movement indexing.

Artifacts

In [12], authors claim that Artifacts are signals recorded by EEG but not generated by the brain. Some artifacts may mimic true epileptiform abnormalities or seizures. Awareness of logical topographic field of distribution for true EEG abnormality is important in distinguishing artifacts from brain waves. Physiologic artifacts originate from the patient and non-physiologic artifacts originate from the environment of the patient.

There are two main categories of EEG artifacts. The first one, which is the most common, includes the biological artifacts generated by sources external to the brain and must be removed during the data analysis and processing. The second category contains externally generated artifacts, mainly environmental, like powerline noise, which can be easily removed during recording through technology [13].

((a)) Clean EEG.

((b)) Pulse.

((c)) Muscle activity.

((d)) Eye movement.

((e)) Eye blink.

((f)) 60Hz line noise.
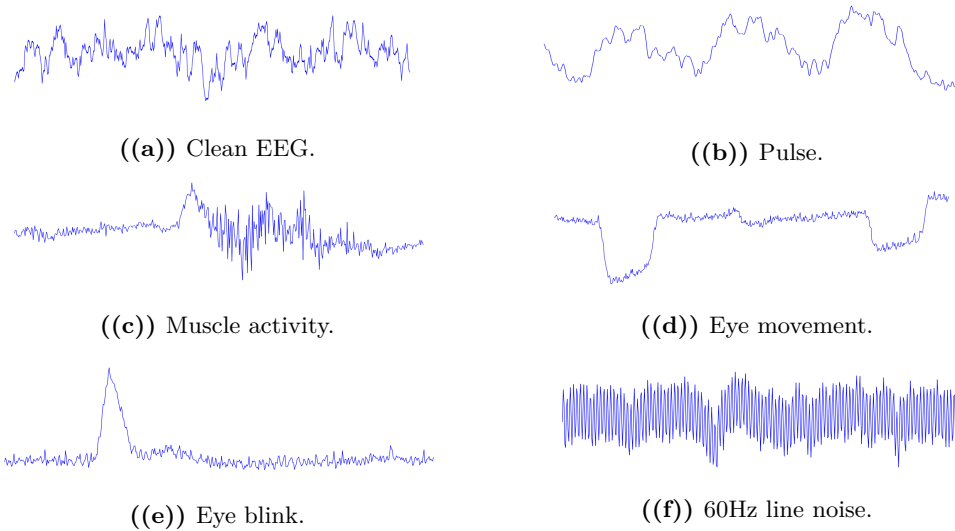
Figure 2.4. Six EEG common artifacts [13].

Physiological artifacts

- The **ocular activity artifacts**, shown in figures 2.4(d) and 2.4(e), might cause significant corruption of the recording signal due to its high-level amplitude, which sometimes can be greater than the signal itself.

However, this feature can be used as an asset, for testing whether the electrodes have been placed properly or not, before recording [14, 15].

- The **muscle activity artifact**, shown in figure 2.4(c), is the electrical activity production of the muscles' contraction. Its interference on the signal can be observed with the naked eye due to the high frequency, thus overlapping in beta and gamma EEG bands is possible. Main factors able to produce that type of artifact are clenching the jaw, talking, chewing, swallowing, and sniffing [14, 15].

- The **cardiac activity artifacts**, shown in figure 2.4(b), are less common as they depend on the subject body shape and electrodes' placement. Their presence is caused by cardiac activity or pulse, and they are a bit difficult to detect and observe because of the EEG signal overlapping [14, 15].

Non-physiological / Technical artifacts
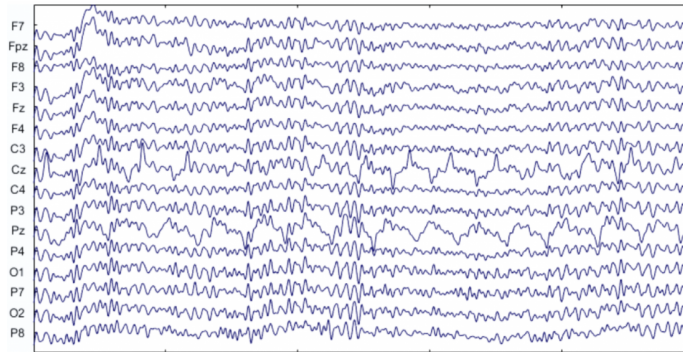
Figure 2.5. Distortion in Cz or Pz appears when moving cables [16].

- The **Cable movement artifacts**, shown in figure 2.5, are mainly caused by cable movement or cable touch that tends to produce distortion, because of the electromagnetic field changes. Based on the movement, either rhythmic or not, their distortions might overlap EEG signals and produce non-EEG-related frequency peaks [16].

- The **Incorrect reference artifact**. This type of artifact, shown in figure 2.6, originates from the misplacement or bad contact of the reference

channel. It can be easily detected on the time domain because of the
sudden changes, in every connected channel, with high amplitude [16].
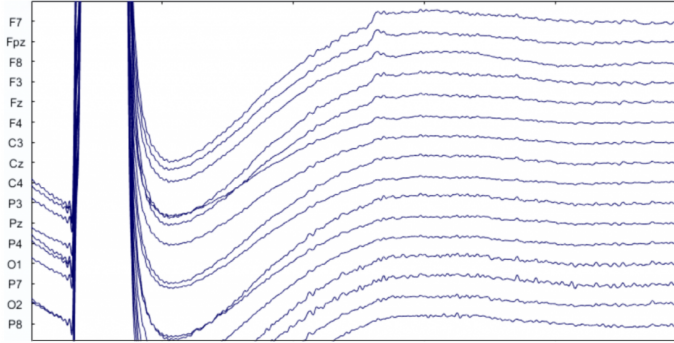
Figure 2.6. High amplitude sudden change in all channels when the reference is not
connected that slowly converge to actual EEG when placed again [16].
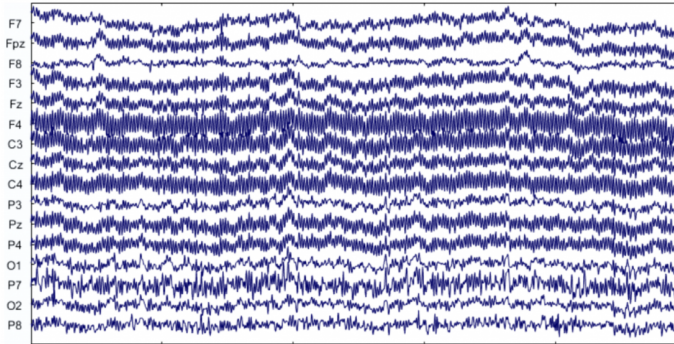
Figure 2.7. High frequency signal overlapping the EEG data in every channel [16].

- The **AC electrical and electromagnetic interferences**, shown in
  figure 2.7, are caused only by the frequency of the power line, which is
  60 Hz for America and 50 Hz for the rest of the world. In addition, they
  are clearly depicted in the corresponding frequencies on the frequency
  domain as a big spike. This type of artifact can lead to severe signal
  corruption due to continuously overlapping, and the reason is the elec-
  tromagnetic fields of AC power source and wires. The application of
  notch filtering in the corresponding frequency becomes necessary [16].

- The **Body movements**, shown in figure 2.8, compose another artifact
  to be mentioned. Understandably arm and head movement, walking or

running affect the contact between electrode and skin, and that leads to signal corruption. In the time domain, temporary slow waves observed consonant with the rhythm of movement [16].
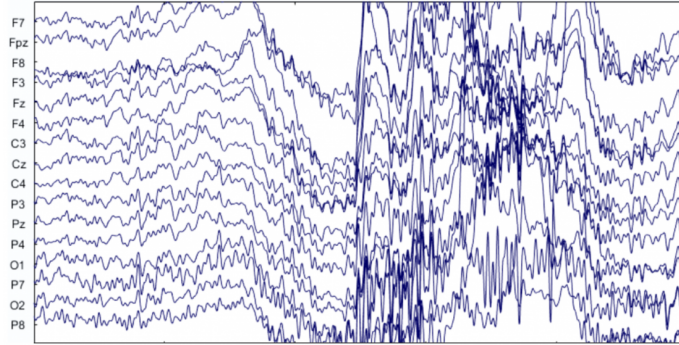
Figure 2.8. The effect of moving the head overlapping the EEG data in every channel [16].

Evoked potentials

They are used for measuring electrical activity in specific locations of the brain and spinal cord. There are two main types, the exogenous and the endogenous. The first one, caused by sensory stimulus, while the second one by thinking or motor processes. The Event Related Potentials (ERP) are voltage changes measured on the scalp, and they are time-locked to the specific event, while, since the middle of the 20th century, forming a significant tool of brain computer interface technology. However, to recognize the ERP components from raw EEG data, they must be obtained in windowed data on a specific recording period after many repetitions, because of their small amplitude [17, 18].

2.3   Signal acquisition

Signal acquisition is the first part of the whole system, consisting of the receiving and registering of generated neural signals before the processing state. The acquisition can be accomplished with three different procedures, invasive, non-invasive, and semi-invasive [19].

- **Invasive**: Placing electrodes directly on the brain through surgery.

- **Semi-invasive**: Placing electrodes in epidural or arachnoid space.

- **Non-invasive**: Placing electrodes on the scalp as described below.

For this research, only Non-invasive electrodes have been used. They are silver or silver chloride conductors that carry current, and in EEG, they are used for receiving and recording detected brain waves by the electrical activity of nerves. In addition, due to the weak signal they receive, there is a need for an EEG machine to amplify them. Both dry and wet electrodes, the two main types of non-invasive ones, were used.

2.3.1   Wet electrodes
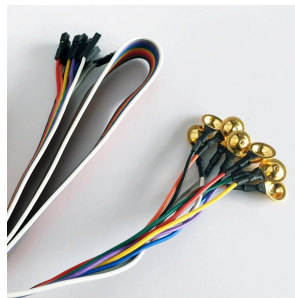
Figure 2.9. OpenBCI gold cup wet electrodes.

It is one of the most widely used types of electrodes, and they are made of silver or silver chloride. In EEG, one of the most important factors for signal acquisition is the impedance between the skin and the electrode, thus it needs to be limited to an acceptable range of 5–20KΩ. In order to achieve optimal impedance and data quality, when using wet electrodes, the use of conductive electrode gel is mandatory. However, the main problem is that the

gel's effectiveness is deteriorated within 5 hours after its application, as it dries. Thus, this kind of electrode is not recommended for long-term use. In addition, using that kind of gel for the electrodes has a lurking risk of creating contact between two or more electrodes when using too many electrodes. Finally, depending on the subject's epidermis, the skin abrasion might result in even better recordings [20–22].

2.3.2 Dry electrodes

Contrary to wet electrodes, the dry ones need no special skin preparation, as they are equipped with micro-needles to closely contact the scalp's conducting layers. The fact that there is no need for the conductive gel when using dry electrodes, makes them capable of long-term experiments and other applications. However, the absence of that gel is the main reason the dry electrodes are more sensitive to noise and interference. To minimize such artifacts, most BCI systems use active dry electrodes carrying an amplifier [20, 21].

- **Active Dry Single Gold Pin-Based Electrodes**

    This type of dry electrode is a single gold-covered pin, which resembles the shape of a mushroom. Its length varies between 10, 12, and 14 mm, to achieve optimal contact despite the subject's hair or scalp site [20].

Figure 2.10. Active Dry Single Gold Pin-Based Electrode [23].

- **Dry Multiple Spikes-Based Electrodes**

    These specific electrodes achieve electrical contact through multiple spikes in a circular shape. Their length varies and might be able to reach up to 3 cm. In addition, there are two types, passive and active ones. The latter integrates an amplifier to limit external signal interference compared to the first one which is directly connected to the EEG amplifier and is more vulnerable to external noise [20].

Figure 2.11. G-tec active dry multiple spikes-based electrode.

Figure 2.12. OpenBCI passive dry electrode.

2.3.3   Comparison between Dry and Wet electrodes

Taking the above into account, dry electrodes are promising contrary to the wet type, as they are more user-friendly and not restricted only in lab and research areas. There is no need for skin preparation and the use of gel in wet might cause dehydration after a long time of usage, which will lead to corrupted signals. However, according to research, the dry electrodes tend to be more sensitive to cable and body movement artifacts, as well as to noise. Furthermore, the results of studies that indicate a 30% lower information transfer rate proves the necessity of improvements needed to be made to completely replace the wet electrodes with dry [21].

2.3.4   Electrodes position
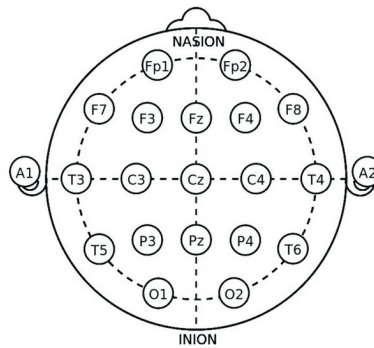
Figure 2.13. The 10–20 International system of EEG electrode placement [24].

In 1958, Herbert H. Jasper invented the "International 10–20 system of electrode placement", as shown in the figure 2.13 [25]. This system consists of 21 positions, resulting by placing adjustment electrodes on a distance of either 10% or 20% of the total Nasion-Inion or ear-to-ear distance of the skull. However, in 1991, the extending 10–20 international system of electrodes was proposed by GE Chatrian, E Lettich, PL Nelson and approved by the American Electroencephalographic Society. That system consists of the 21 primary electrodes of Harbet's and 54 secondary ones as shown in the figure 2.14 [5].

The electrode placement is partly named after the first letter of the brain area they are adjusted to, Frontal, Central, Temporal, Posterior, Occipital. Along with the letter, a number is given depending on the point of view of the subject. On the midline, the area letter is accompanied by the letter 'z', at the left area, by odd numbers, while at the right one by even numbers [5].
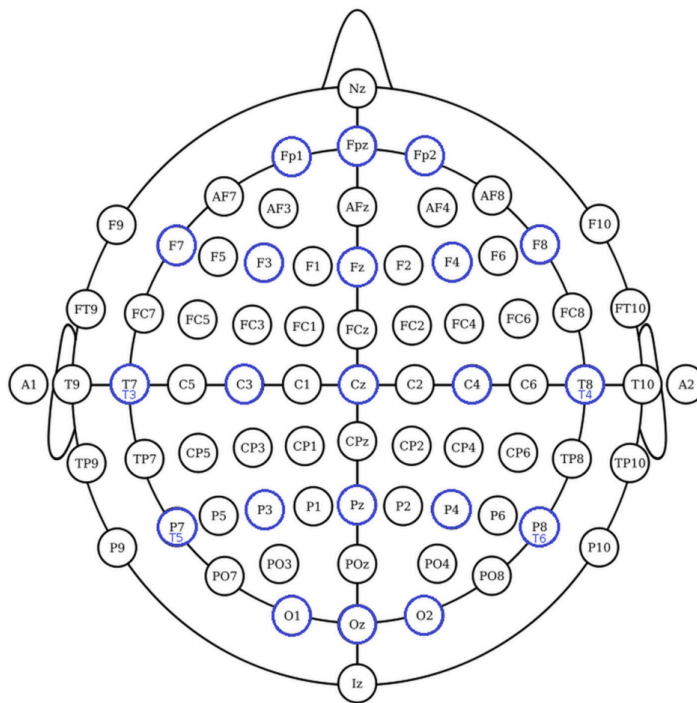
Figure 2.14. The extended 10–20 International system of EEG electrode placement. Blue circles represents the location of 10–20 EEG electrodes [26].

2.4   Brain computer interface
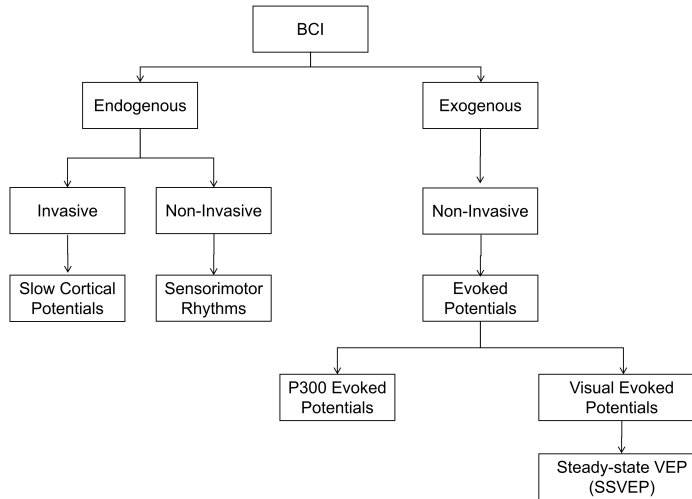
Figure 2.15. Types of brain signals used in BCI.

BCIs make it feasible to pass the electrical signals which originate from the brain, to an external system that in turn analyzes and translates the generated signals into commands to fulfill specific tasks. Moreover, BCIs prove to be an opt tool for paralyzed people because there is no need of any connection with muscle or neuromuscular parts as they focus on brain impulses. Their usage ranges from medical applications for movement and communication disabilities and may extend to healthy people in need of hands-free devices. There are no limits to their promising applications till today.

There are three main types of brain signals as shown in figure 2.15.

- **Slow Cortical Potential (SCP)**

  Slow cortical potentials are potential shifts that occur over 0.5–10.0 seconds. Positive SCPs are usually related to decreased cortical activation, whereas negative SCPs are usually associated with increased cortical activation, e.g. movement.

- **Sensorimotor Rhythm (SMR)**

  The SMR is an oscillatory idle rhythm of synchronized electric brain activity, and its frequency ranges between 13 and 15 Hz for most people.

The SMR has been widely used in BCI systems, nevertheless, compared to SSVEP-based BCIs, SMR-based BCI require much longer training periods, they can offer a limited number of targets, and they achieve lower levels of accuracy [27].

- **Evoked Potential (EP)**

  They are used for measuring electrical activity in specific locations of the brain and spinal cord. Additionally, they are divided in Visual evoked, like SSVEP, and P300 Evoked, with the first providing higher accuracy and ITR. Moreover, SSVEP-based systems require less training time and fewer EEG channels.

2.4.1   SSVEP

SSVEP is the measured brain potential that arises spontaneously when a prolonged oscillating visual stimulus is observed. At the frequency of the stimulus oscillation, the measured potential has a distinct spectral component.

In SSVEP-based BCI systems, these distinct spectral components are used for distinct commands for a controlling system, after data filtering, feature selection and feature classification. In this research, four targets were used for the visual stimuli, each one of them flickering on a different frequency. Each one of the frequencies, as well as their harmonics, are used for the navigation system to initiate different commands.

Since the system being analyzed is related to navigation systems for people with mobility problems, it needs to be accurate as much as possible and, at the same time, have a quick response to the user's commands. As a result, for this research, SSVEP based BCI was used instead of Event-Related potentials, like P300, or Slow Cortical Potentials. Contrary to these alternative modalities for BCIs, the SSVEP outperforms due to less user training time, higher Information Transfer Rate (ITR), and greater accuracy. The ITR is a metric used for evaluating BCIs' and other control systems' performance, and it describes the amount of data transferred per unit of time.

SSVEP is a frequency coded brain response modulated by the frequency of periodic visual stimuli higher than 6 Hz [28]. It is one of the most sound real-time BCI applications, due to ease of use, the high SNR and its low susceptibility to Artifacts [29]. The main electrodes, used in SSVEP, are placed in the posterior and the occipital part of the brain because the continuous visual stimulation evokes a precisely synchronized brain activity depending

on the user's selective focus on one of the flickering patterns. The flickering pattern's fundamental frequency, as well as its harmonics, can be spotted on the SSVEP.

According to the study [30], using CCA in SSVEP based systems increases ITR. However, detecting patterns in freely moving human case studies using CCA is not as effective once walking speed increases, probably due to intense existence of head-movement artifacts [28, 31].

2.5   Data processing algorithms
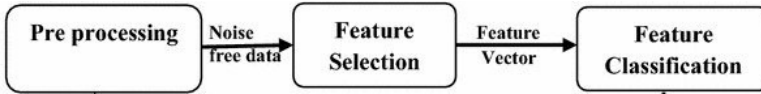
Figure 2.16. Processing model in EEG-based BCI system [32].

In order to use SSVEP based system for online experiment purposes, the subject needs to undergo a training season. Usually, the SSVEP system uses one algorithm for signal enhancement and one for data classification to train the system to recognize the class of the receiving EEG signal.

In the preprocessing stage, the training data are usually filtered with band-pass filtering, and depending on the strength of AC electrical and electromagnetic interferences, it might need to apply notch filtering. Another preprocessing procedure is other artifact noise removing like those coming from eye blinking and muscle movements. This procedure was not used in this research.

For the feature selection in SSVEP based BCI systems, various techniques can be used, like FFT-based algorithms, CCA, Independent Component Analysis (ICA), Power Spectral Density (PSD), and wavelet transform. Even though most of SSVEP based BCI system using the ICA, this research used the CCA as it can provide better accuracy and ITR according to [32].

As far as the feature classification is concerned, the LDA algorithm was preferred contrary to Support Vector Machine (SVM) and K-Nearest Neighbor (KNN) for two main reasons, accuracy and processing time. According to research [33], the LDA is slightly more accurate than SVM, but it needs much less processing time compared to both SVM and KNN in multi-class classification. SVM needs almost 44 times the LDA's processing time, while KNN takes double the LDA's time.

2.5.1   CCA

CCA is the statistical method that tries to maximize the possible underlying correlations between two sets of data. In EEG, the calculated correlation coefficient is between the electrodes and the reference signals. The correlation between the canonical data is maximized through a calculated linear combination according to formula 2.1.

$$
\begin{aligned}
max_{W_x,W_y}\rho(x,y) &= \frac{E\left[x^T y\right]}{\sqrt{E\left[x^T x\right] E\left[y^T y\right]}} \\
&= \frac{E\left[W_x^T XY^T W_y\right]}{\sqrt{E\left[W_x^T XX^T W_x\right] E\left[W_y^T YY^T W_y\right]}}
\end{aligned}
\tag{2.1}
$$

,where X, Y are random variables and x,y are their linear combinations, respectively. So, by solving formula 2.1, CCA finds the ideal weight vectors W_x and Wy to get the maximum correlation between X and Y.

2.5.2   LDA

LDA is a technique that focuses on maximizing the separability among specific categories for making easy decisions. It is achieved by maximizing the distance between the projected mean values of the found hyperplane and minimizing the interclass variance between the data.

Figure 2.17 clearly shows that different classes have moved away from each other as much as possible, but at the same time, the categorical data have come closer to each other [34]. It is a beneficial tool for dimensionality reduction problems as a pre-processing step for machine learning and pattern classification applications.

To solve this problem, probability, mean value, and covariance matrices are calculated for each one of the classes. Then, follows the calculation of the scatter matrices for each class S_W and between class S_B according to the following mathematical formulas.

$$
S_W = \sum_{i=1}^{c} P_i \Sigma_i \qquad\qquad S_B = \sum_{i=1}^{c} P_i(\mu_i - \mu_0)(\mu_i - \mu_0)^T
$$

Where c is the number of classes P_i S_i and μ_i, the probability, the covariance matrix, the mean value of each category, and μ_0 is the mean value of

all data. Since one of the major problems is to maximize the distance among every class, this leads to maximizing over the total mean value μ_0. Finally, the projection matrix comes from the solution to the following generalized eigenvalue problem.

$$S_W^{-1} S_B W = \lambda W$$
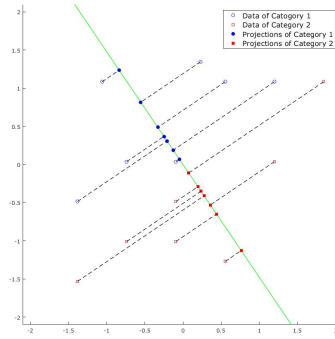
((a)) LDA data and hyperplane projections of two different classes.
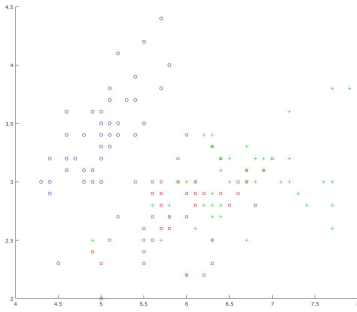
((b)) Data plot of 3 different classes before LDA application.
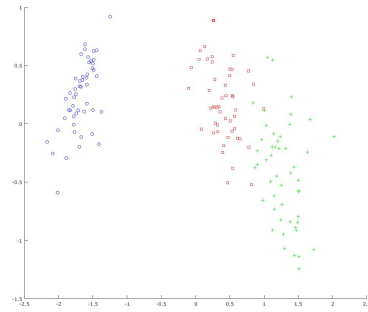
((c)) Data plot of figure 2.17(b) after LDA application.

Figure 2.17. LDA application for 2 and 3 different classes.

CHAPTER 3

Related work

This thesis is based on the research "Single-Channel SSVEP-Based BCI for Robotic Car Navigation in Real World Conditions" [1]. It is an SSVEP-based BCI system with average offline accuracy of 81%. The brain signals coming from the occipital lobe are recorded and the detecting frequency and harmonics of the flickering targets are translated into commands for controlling a robotic device. The main asset of this research compared to the above mentioned is the usage of a camera on the robotic car allowing live video feedback. Furthermore, only one electrode on the visual cortex is used, in a different location for each subject, depending on the lowest impedance. In addition, the experiment was conducted in a noisy and non-isolated environment, simulating real life conditions. Lastly, the data analysis used the CCA algorithm, and the results showed that in association with LDA classifier can give 117.1 $bits/min$ mean value of ITR during the online experiment, which is considered higher than the average.

3.1 Proposed project approach

This thesis attempts to develop a BCI system similar to prementioned one by placing two more electrodes and using a less costly electroencephalograph for data acquisition. The goal is to create a system less costly in hardware thus making it competitive to other costly technology like g.MOBIlab+, using trending algorithms such as CCA and LDA.

CHAPTER 4

Methodology

4.1 Design of SSVEP system

4.1.1 Architecture of the system
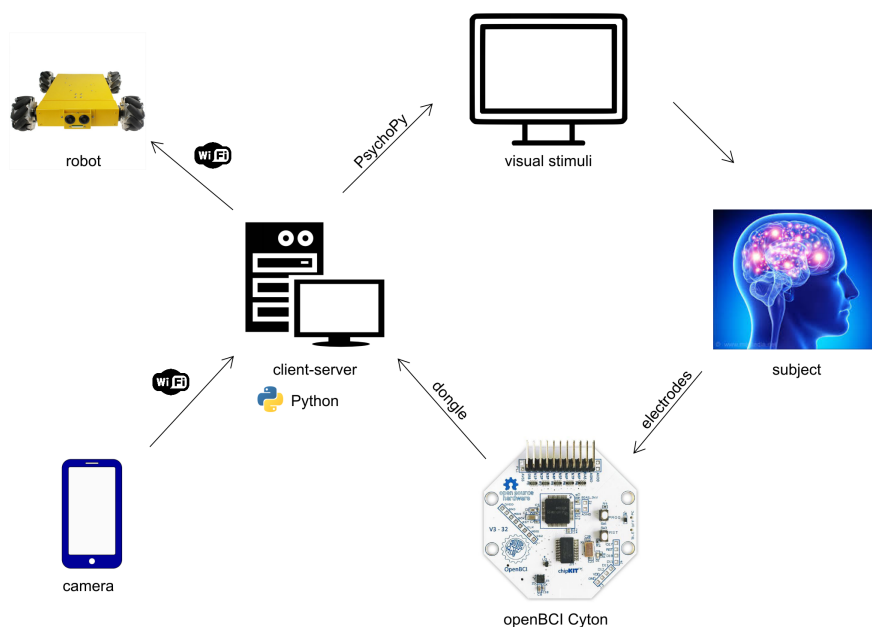
Figure 4.1. Architecture of the SSVEP system.

Figure 4.1 describes the architecture of the integrated SSVEP-based BCI system. More specifically, as long as the participant is gazing at a specific target of the visual stimulus interface, the openBCI Cyton board captures the brain activity of the occipital lobe through electrodes. At the same time, the Cyton board is sending the collected data to the client-server module, which in

turn, using dedicated processing algorithms, detects the target, at which the participant is possibly gazing. The detected command is being transferred to the nexus robot through Wi-Fi protocol. During navigation, a mounted camera on the robot is continuously sending video feedback to the user, which is integrated into the visual stimulus interface.

Client-server
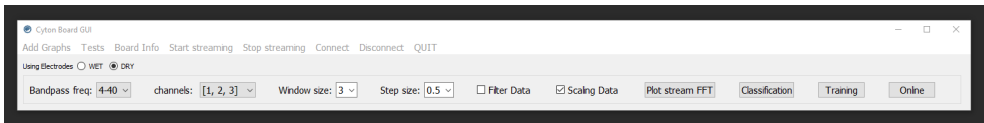
Figure 4.2. The GUI developed for the thesis' experiment purposes.

The client-server is the main program, running through the GUI, depicted in figure 4.2, which has been developed for the thesis' experiment purposes, using python and the PyQt5 package. Through the GUI, the user can control the OpenBCI Cyton Board, the training and online sessions used in the experiments, and plotting various graphs, e.x. time-series graphs. More specifically, the GUI supports:

1. Board handle

   a) Connect to board.

   b) Disconnect from the connected board.

   c) Start streaming data from the connected board.

   d) Stop the running streaming.

   e) Get the connected board's configuration.

   f) Run some tests given by the OpenBCI developers.

   g) Choose whether the received channel data will be filtered and scaled according to the amplification scale factor.

2. Set streaming variables

   a) Connected channels on board.

   b) Choose the connected type of electrodes.

3. Set processing variables

    a) Choose the bandpass filter frequencies.

    b) Change the window size and the step size for the signal packages.

    c) Choose the channels for the recorded data that will be used in the processing.

4. Add graphs for live signal observation (FFT, Time series)

5. Plot an FFT graph for a given streaming session, chosen via file dialog.

6. Create a classifier for the online session for the given training sessions in the open file dialog.

7. Start training session.

8. Start online session.

Finally, this module is responsible for receiving the data from the Cyton board, analyzing-classifying them, and predicting the following command sent to the nexus robot through the running python program.

Visual stimuli
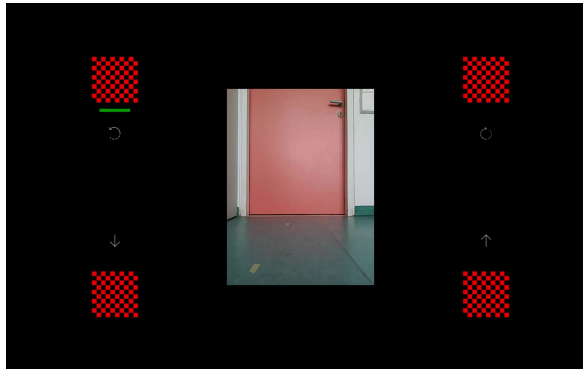
Figure 4.3. SSVEP interface display.

For the SSVEP stimulus generation, an interface similar to the one developed in the experiments of research [1] and depicted in figure 4.3 was used. More precisely, four flickering checkerboards got equally allotted in the equal

number of edges of a 1920x1080 and 60Hz of refresh rate screen monitor. The prementioned interface was developed in python, using the "PsychoPy" [35], a free cross-platform package for running experiments in the behavioral sciences. Each target is flickering on a different frequency and, more specifically, the upper right on 3 Hz, the upper left on 3.75 Hz, and the two lower targets, on 3.33 Hz and 4.28 Hz, for the left and right corner, respectively. Moreover, the corresponding commands for each flickering target are left, right, back, front, in the order previously mentioned, and the stop command refers to every other screen point apart from the flickering targets. For the two different experiment's sessions, training and online, the interface works differently, explained below in sections 4.2.2 and 4.2.4.

OpenBCI Cyton board

The openBCI Cyton V3-32 board (figure 4.4) is equipped with bio-signal amplifier System On a Chip (SoC), the ADS1299, responsible for recording 24bit signals from up to eight different channels. Right after receiving the channel data, they are moved to a PIC32 microcontroller, which in turn the data will be sent to the RFduino, a radio-enabled microcontroller, through serial communication bus. The RFduino is responsible for wireless data transmission. The board itself is capable of transmitting data up to 250 samples per second, in three different ways, via dongle picturing in figure 4.5, Bluetooth Low Energy (BLE) communication, and even through Wi-Fi, providing the Wi-Fi shield board is connected. Finally, this board can be used for EEG, Electromyography (EMG), and Electrocardiogram (ECG) [36].
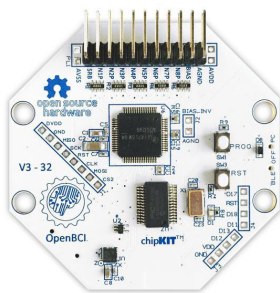
Figure 4.4. OpenBCI Cyton V3-32 board.
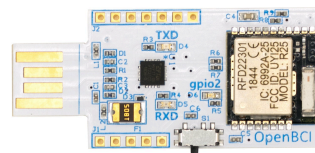
Figure 4.5. OpenBCI USB dongle.

Robot

In the online session of the experiment, the evaluation of the SSVEP system's accuracy performed using "4WD MECANUM WHEEL MOBILE ARDUINO ROBOTICS" by Nexus Robot, figure 4.6 [37]. For the robot handling, two microcontrollers were used. More specifically, an Arduino Due for the wireless communication was used via Wi-Fi with the client-server module receiving each sending command and forwarding it to the Arduino 328 Controller, the microcontroller for the motors handling.

Figure 4.6. The 4WD robot used in the experiment.

Camera

An android smartphone mounted on the robotic car was used for the live video feedback in the online session. The phone runs an application simulating an IP camera, streaming on the phone's IP address. So, to have the live video in the visual stimuli interface, the client-server module creates wireless communication through Wi-Fi with the smartphone.

4.1.2   Data acquisition

The aim of this research is to make an accurate system with as few electrodes as possible. So the whole experiment took place for both wet and dry electrodes using four channels on points O_1, O_z and O_2. However, in order to check the variation in the system's accuracy using one more channel, four in total, five representative participants were chosen to repeat only the training session with an extra channel placed on PO_z.

Wet electrodes

Four OpenBCI Gold Cup Electrodes (figure 2.9) were used for the data recording during the first half of the experiment. Firstly, each subject's skin got abraded very carefully to remove most of the dead cells from the epidermis and accomplish the very best contact between electrodes and head. Then, after filling electrode paste into white gold cup electrode, they were placed, according to the extended international 10–20 system (figure 2.14), on points O_1, O_z, O_2 and PO_z. The ground electrode was placed in the F_{pz} point while the reference one was on either one of the subject's earlobes.

((a)) g.GAMMAcap².

((b)) g.SAHARAbox.

((c)) g.SAHARAelectrode.
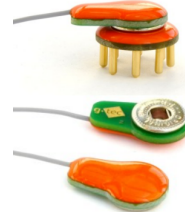
((d)) g.SAHARAclip.

Figure 4.7. G.SAHARA active dry electrode system.

Dry electrodes

For the dry electrodes, two different technologies were tested, passive and active, and in both cases four electrodes were used, placed on O_1, O_z, O_2 and PO_z.

The first one was the openBCI passive dry electrodes depicted in figure 2.12. In preparation for the experiment, the first tests during the trial training session, the accuracy was not acceptable ranging from 35% to 40% and on account of this were not used in the official experiments.

The second type of dry electrodes, the g.SAHARA active dry electrode system, produced better accuracy and was used for the experiments. The

asset of this one, contrary to openBCI's, is that it uses the g.SAHARAbox (4.7(b)), as the power supply for the active clips and converts them to conventional passive EEG connectors. This module amplifies the incoming signal, and therefore the impact of ambient electrical noise may get reduced significantly. Finally, the g.GAMMAcap² was used to place the active dry electrodes properly on the head, and both versions of electrodes, standard (7mm) and long pin (16mm), depicted in figure 4.7(c) were used for short and long hair, respectively.

4.2 Experiment

In order to verify and evaluate the proposed SSVEP system, an experiment of three parts was performed. The participants underwent the specific experiment twice, so as to compare the usage of both electrodes, wet and dry.

4.2.1 Description

Ten participants, five males and five females with ages ranging from 23 to 47 years old, voluntarily participated in this experiment. Prior to the experiment, all participants were fully informed of the procedure and purpose of the experiment and their permission was asked to store and process their data, according to the General Data Protection Regulation (GDPR). In addition, they confirmed that they do not suffer from any medical condition that may put them at risk during the experiment, such as epilepsy. Finally, the experiment was divided into three parts, the training, the testing and familiarization of the system, and the online.

The participants were seated in a noisy office area under normal light at a distance of 70cm from the visual stimuli monitor in the duration of all three sessions.

4.2.2 Training session

This part focuses on the system's training. Before starting the training part, in order to verify that the electrodes were placed correctly and that there is not too much corrupting noise, the receiving signals were checked for alpha band signals and muscle activity artifacts. For the alpha band, the participants were requested to stay restful with closed eyes, while for detecting the muscle

activity artifact, they were asked to grit their teeth. Results of a representative participant are shown in figures 4.8 and 4.9.
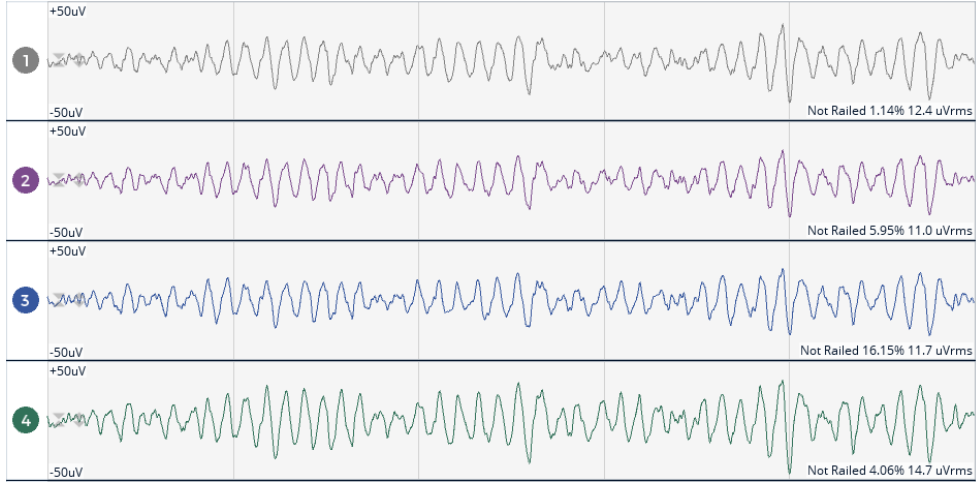
((a)) Time series plot.
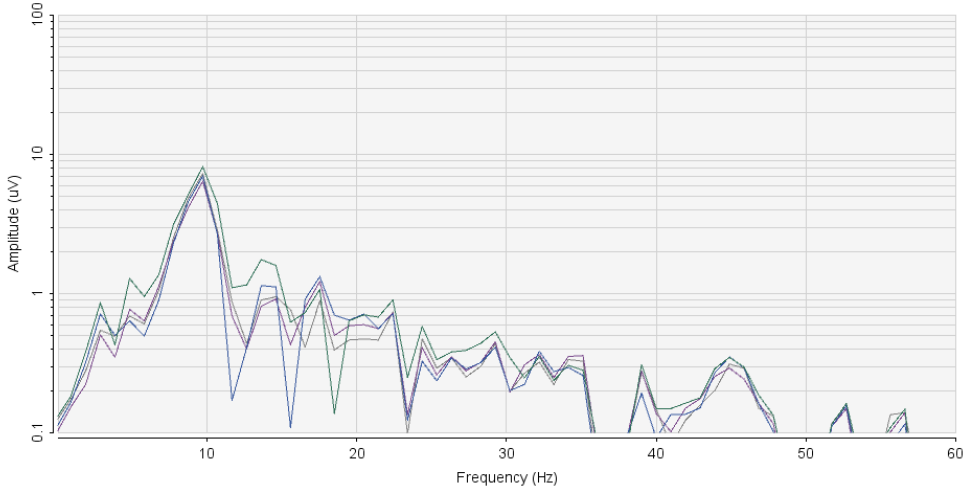
((b)) FFT plot.

Figure 4.8. Detected alpha band in participant's signal, using Dry electrodes. Notch filtering in 50Hz has been applied.

Figure 4.8(a) clearly shows the normal activity of alpha-band as expected and depicted in figure 2.3, while the FFT plot in figure 4.8(b) shows an intense activity in 10 Hz which is the mean value of the alpha band frequency range.
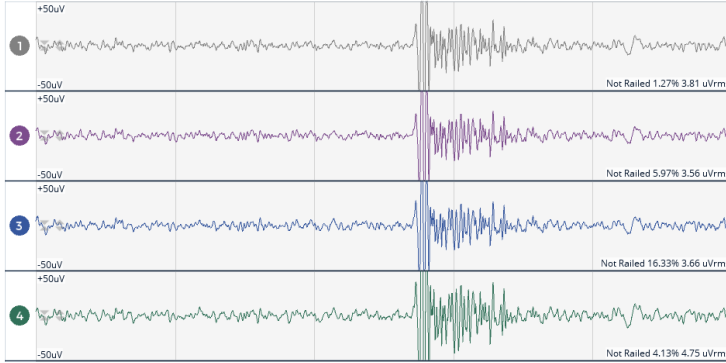
((a)) Time series plot.
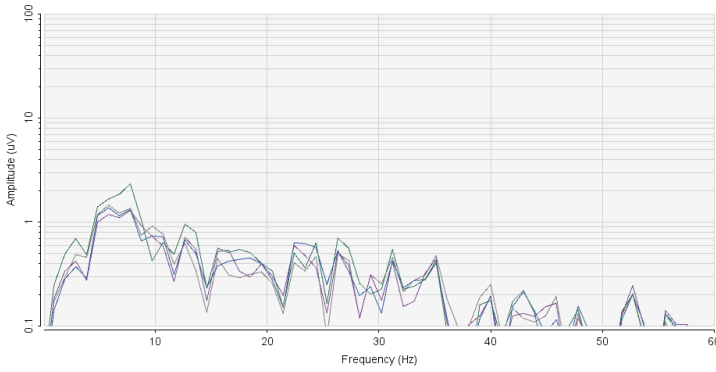
((b)) FFT plot.

Figure 4.9. Detected muscle activity artifact in participant's signal, using Dry electrodes. Notch filtering in 50Hz has been applied.

Another point to pay attention to while testing the electrodes is the FFT plot. This one gives a good view of their application and the amount of noise present in the recording signals. More specifically, all three figures 4.10, 4.11 and 4.12 clearly show intense activity in delta (0.5-4Hz), theta (4-8 Hz), alpha (8-14 Hz), and beta (14-30Hz) bands which are four of the five main frequencies measured by EEG. Moreover, the notch filter eliminates the ac artifacts when using dry electrodes, as figure 4.10 clearly shows at 50 Hz. Figure 4.12, proves that despite the existence of ac artifacts in 50 Hz, it is not in that high amplitude to be destructive for the receiving EEG signals, contrary to cases using dry electrodes that the ac artifacts are dominating, as depicted in figure 4.11. This observation was more than expected based on other related works using dry electrodes, which refer that the dry electrodes are tended to

be more sensitive to AC artifacts.
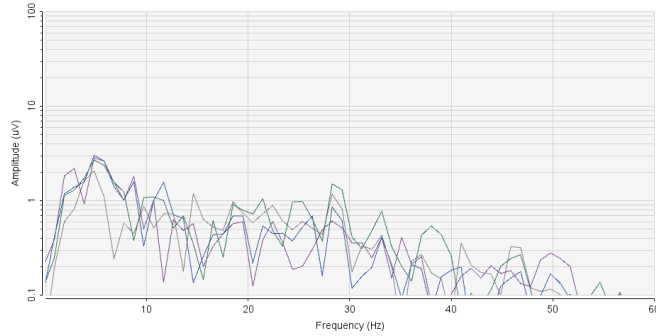
Figure 4.10. FFT plot of receiving signal using dry electrodes. 50Hz notch filter is applied on the signal.
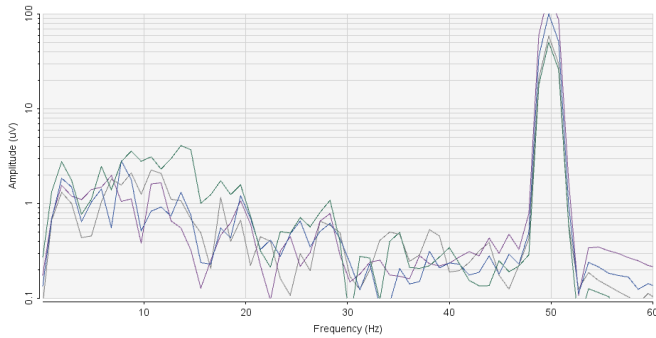
Figure 4.11. FFT plot of receiving signal using dry electrodes. No filtering applied.
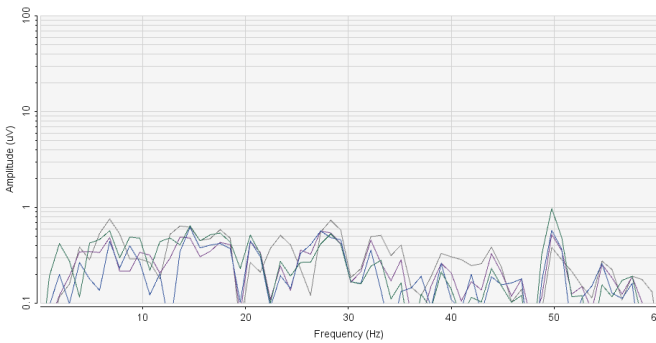
Figure 4.12. FFT plot of receiving signal using wet electrodes.

After testing the electrodes, the training session starts. More specifically, in order to lead the system to identify the target, which the participant is gazing at during the online session, a dataset of valid signals is needed to be created. To achieve this, the participant is requested to gaze continuously at only one target per specific time duration, set to 7 seconds for this experiment. During the training session, for the four checkerboards-targets, the system guides the participant following a white arrow to stare at a specific one, as shown in figure 4.13. For the fifth command, which is the center of the interface, a white square is displayed in the center. Finally, the system's training consists of four independent training sessions that, in turn, consist of a pattern in which the user is gazing at each of the four checkerboards three times (21 seconds) and the center target four times (28 seconds). The command of the center target is the STOP, so the system needs to have more samples for better accuracy and safety reasons.
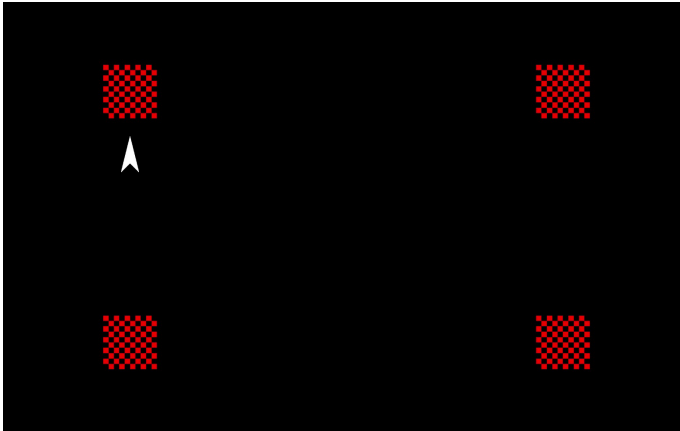
Figure 4.13. Visual stimuli interface during training session.

4.2.3   Testing session

During this session, the participants have the opportunity to test the SSVEP system in order to familiarize themselves with the commands and the online session's interface before starting the online experiment. This session has been added because in the first trial tests in the laboratory, it was observed that once using the wet electrodes after the dry ones, the participants followed the predefined route for the online experiment more easily and quickly. Therefore,

the participants undergoing the same experiment first with dry electrodes and then with the wet electrodes, were becoming familiarized with both systems.

4.2.4 Online session

It is important to mention that in order for the participant to be able to navigate the robot using both dry and wet electrodes, the training accuracy needed to be above 70 percent otherwise, it was challenging and sometimes impossible for the system to detect at which target the participant is gazing at and as a result the navigation was unattainable. During the online session of the experiment, the participants drove the robot in a specific predefined route inside the lab, as depicted in figure 4.15. Moreover, in order to collect data for every possible system command during the drive, the participant was asked to use the Back command. Therefore, the participant continued driving backward after reaching the black cross until the red one, as shown in figure 4.15. During the whole session, participants used the camera video feedback in the center of the interface to navigate the robot on the predefined route, figure 4.14. Finally, a green line was printed under or next to the target the system predicts as the given command. In this way, both the user and the researchers were able to verify whether the system predicts correctly the desired command or not.
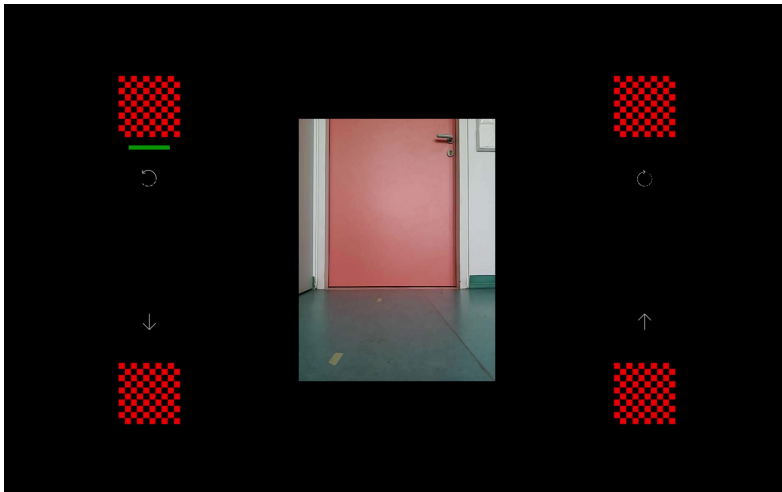
Figure 4.14. Visual stimuli interface during online session.
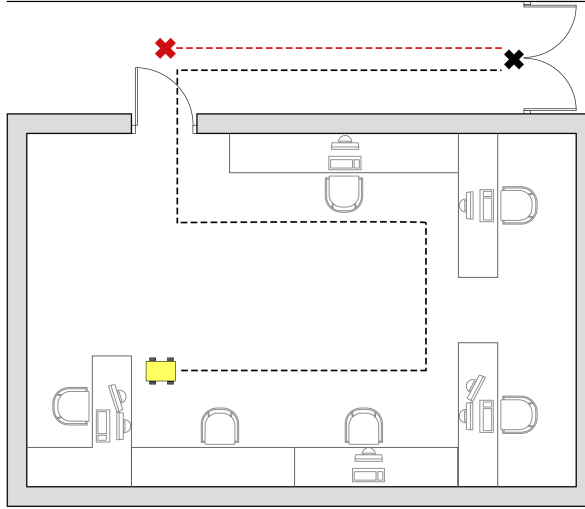
Figure 4.15. The predefined route used for robot driving during the online session. For the black route, the forward command is used while the backward command is used for the red one. The red cross shows the finishing point.

4.3   Detection of the SSVEP response

During the training session of the experiments, to ensure that the obtained data were acceptable, a FFT plot with the recorded signals was created using python. A noteworthy example of such a graph presented in figure 4.16 clearly shows the second and the fourth harmonic of 3.33 Hz stimuli. Furthermore, the SNR and the frequency of the highest amplitude are reported in the plot, so as to inform whether the second harmonic has the highest peak or not. For the FFT plot, the received signal got filtered with a 5th order Butterworth bandpass filter between 4–40 Hz, and a notch filter in 50 Hz, to remove AC electrical and electromagnetic interferences.

The recorded signals underwent specific processing for their classification using CCA and LDA algorithms. Firstly, signal segments for each channel according to a particular time length (window size), in this research is 3 seconds,
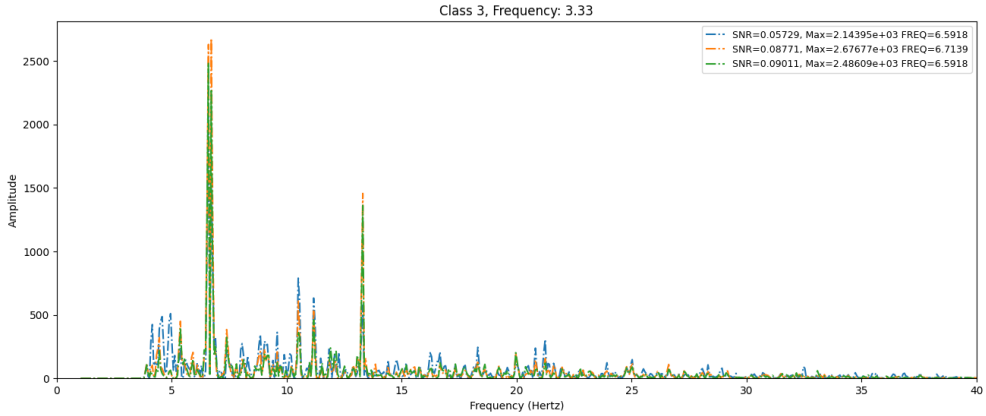
Figure 4.16. FFT graph, presenting data recorded during training session, using g.SAHARA active dry electrode system for 3.33 Hz stimuli.
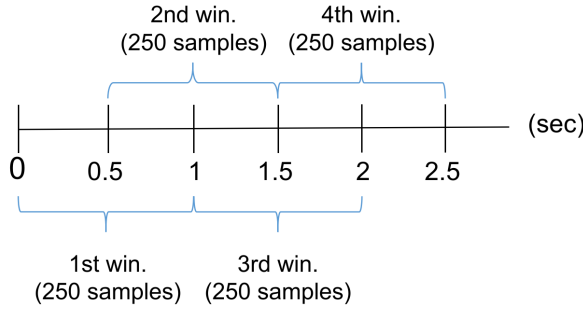
Figure 4.17. Data packages for window size $n = 1$, step size $s = 0.5$ and sampling Rate $= 250$, each window contains $n \times f$ samples, where n is window size in seconds, and consist of both new and old samples with the given step.

are created with new and old data overlapping according to step size, in this case 0.5 seconds. Figure 4.17 is an example of data windowing for window size equal to 1 second, step size 0.5 seconds, and sample rate 250 Hz. Hereupon, there is a different approach for each kind of electrode. More specifically, tests showed that since the dry electrodes are more sensitive to artifacts and mainly to AC electrical and electromagnetic interferences, a notch filter needs to be applied in 50 Hz frequency while wet ones showed that the difference is imperceptible when applying the particular type of filtering. At this point, the data are being filtered with the same bandpass filter used in the case of FFT, for both wet and dry electrodes. Then, the canonical correlations for

each segment have to be calculated as described in section 2.5.1, in order to be used as input for the LDA classifier. The two variables used in the CCA algorithm are x, the collected SSVEP signals, and y, the reference signals for each frequency independently arising from the below mathematical formula 4.1

$$y = \begin{pmatrix} sin(2\pi ft) \\ cos(2\pi ft) \\ \vdots \\ sin(2\pi N_h ft) \\ cos(2\pi N_h ft) \end{pmatrix}, t = \frac{1}{f_s}, \frac{2}{f_s}, \ldots, \frac{N}{f_s} \tag{4.1}$$

, where N is the number of samples, N_h is the number of harmonics, here is 2, f the frequency for the corresponding flickering target, and f_s the sampling rate, here 250Hz.

Results

For the system's evaluation, four different metrics were used. Firstly and most important is the accuracy of the system, calculated with python using the sklearn machine learning library. The training data were split into random train and test subsets, of 65% and 35% of total data, respectively. The second metric is the ITR. Since the system is intended primarily for daily use by a person with mobility problems emphasis is placed on commands' response time which is the third metric. Finally, the total time for completing the predefined route was calculated for each one of the participants.

The ITR was calculated based on the equation 5.1.

$$ITR = \frac{60}{T}C_N \left(log_2 N + P log_2 P + (1 - P) log_2 \left[\frac{1 - P}{N - 1} \right] \right) \qquad (5.1)$$

In the equation 5.1, N is the number of the used targets, P is the LDA accuracy for the testing session, T is the total duration of the session, and C_N is the total number of the classification during this session. During this training session, the used targets are five (N=5), the total duration is T=112 seconds (5 targets × 3 trials × 7 seconds/target + (1 extra stop target × 7 seconds)), and the total number of classification is the same as the total windowed data, in each training session's saved dataset, $C_N = 219$.

The first two tables 5.1 and 5.2 present the first three metrics, for the online experiment as described in subsection 4.2.4. These results are collected with the electrodes placed on O_1, O_z, O_2 and the subjects that were not able to drive the robot, due to low accuracy in training session, pointed with dash in the Total time column of the tables.

Participant ID	Accuracy	ITR (bits/min)	Total time (min)
1	0.9831	253.98	05:33.89
2	0.9888	259.35	03:34.14
3	0.8588	170.35	05:24.39
4	0.7684	126.45	03:23.19
5	0.9719	244.15	03:58.58
6	0.9492	226.46	03:28.74
7	0.9718	244.02	03:43.23
8	0.9718	244.02	03:35.69
9	0.9885	259.09	04:17.63
10	0.9887	259.29	03:49.02
Mean	0.9441	228.71	04:04.85
SE	0.0231	14.15	00:14.91

Table 5.1. BCI Performance using wet electrodes. Electrodes placed on O_1, O_z, O_2

Participant ID	Accuracy	ITR (bits/min)	Total time (min)
1	0.6742	89.12	-
2	0.9774	248.83	08:00.09
3	0.9096	199.84	06:09.94
4	0.7443	116.20	05:41.49
5	0.8418	161.38	05:49.93
6	0.4157	20.41	-
7	0.9318	214.28	04:26.62
8	0.8483	164.78	05:07.89
9	0.8362	158.48	05:59.44
10	0.8701	176.54	06:49.35
Mean	0.8049	154.99	06:00.59
SE	0.0514	20.79	00:22.69

Table 5.2. BCI Performance using dry electrodes. Electrodes placed on O_1, O_z, O_2

Moreover, tables 5.3 and 5.4 show the variation of the algorithm's accuracy and ITR for both dry and wet electrodes based on the used channels. More specifically, each one of the channels in the table was placed in the participants' heads on a specific point, $1 \rightarrow O_1$, $2 \rightarrow O_z$, $3 \rightarrow O_2$, $4 \rightarrow PO_z$, according to the extended international 10–20 system in figure 2.14. Table 5.3 shows the variation for the channels 1,2,3 that used on every participant during the whole experiment, while table 5.4 shows the variation for the channels 1,2,3 and 4

that used only on five representative participants for statistical purposes.

Channels	Dry Accuracy	Wet Accuracy	Dry ITR (bits/min)	Wet ITR (bits/min)
1	0.6452	0.4660	89.75	33.90
2	0.6585	0.3813	91.88	17.75
3	0.6415	0.3024	82.28	7.25
1,2	0.7575	0.8363	130.45	173.23
1,3	0.7445	0.8814	126.51	193.49
2,3	0.7472	0.9203	131.24	212.58
1,2,3	0.8049	0.9441	154.99	228.71

Table 5.3. Mean accuracy and ITR across 10 participants using all possible channel combinations for channels 1, 2, 3, for both types of electrodes. Channels positions are $1 \rightarrow O_1$, $2 \rightarrow O_z$, $3 \rightarrow O_2$

Channels	Dry Accuracy	Wet Accuracy	Dry ITR (bits/min)	Wet ITR (bits/min)
1	0.5921	0.4421	73.73	29.34
2	0.6672	0.3528	95.32	14.04
3	0.6625	0.2681	86.59	5.28
4	0.6725	0.5477	104.61	58.03
1,2	0.7905	0.7921	137.57	153.93
1,3	0.8039	0.8294	144.85	168.97
1,4	0.7157	0.8194	119.16	153.53
2,3	0.7575	0.8936	133.93	197.12
2,4	0.7509	0.8710	136.10	179.55
3,4	0.7948	0.9207	148.59	210.06
1,2,3	0.8584	0.9152	173.07	211.84
1,2,4	0.8448	0.9378	168.73	219.90
1,3,4	0.8503	0.9389	171.09	222.27
2,3,4	0.8526	0.9287	178.31	217.27
1,2,3,4	0.8912	0.9536	195.07	232.70

Table 5.4. Mean accuracy and ITR across the 5 representative participants using all possible channel combinations for channels 1, 2, 3, 4, for both types of electrodes. Channels positions are $1 \rightarrow O_1$, $2 \rightarrow O_z$, $3 \rightarrow O_2$, $4 \rightarrow PO_z$

For better data visualization, the accuracy and the ITR data for both tables 5.3 and 5.4 plotted in the below graphs. Figure 5.1 depicts the accuracy variation for table 5.3, while ITR for the same table is presented in graph 5.3. Finally, the data of table 5.4, are plotted for the accuracy and the ITR in graphs 5.2 and 5.4, respectively. For each one of the figures below, the error bars are the standard error of the corresponding mean values.
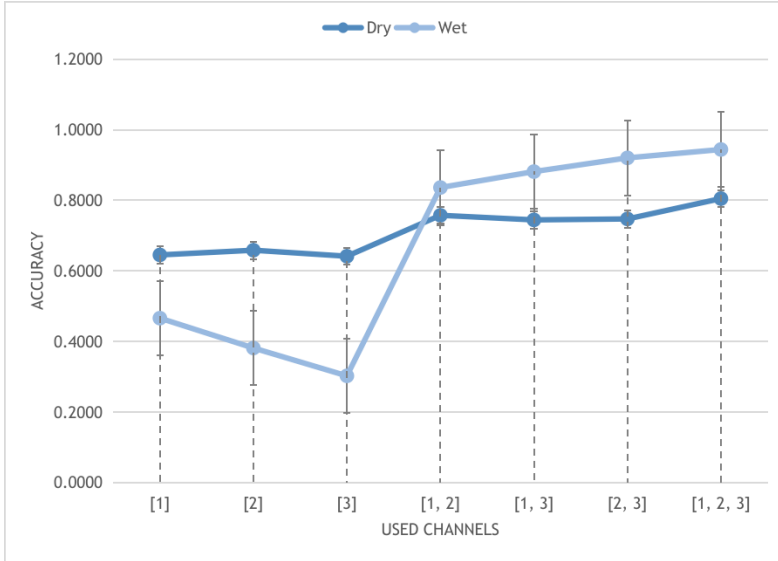
Figure 5.1. Line chart of mean accuracy across 10 participants using all possible channel combinations for channels 1, 2, 3, for both dry and wet electrodes. Channels positions are $1 \rightarrow O_1$, $2 \rightarrow O_z$, $3 \rightarrow O_2$. Data from table 5.3.
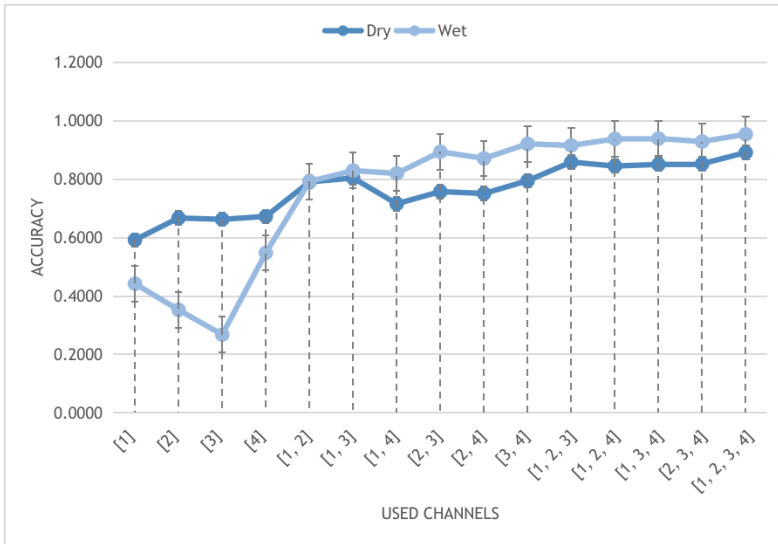
Figure 5.2. Line chart of mean accuracy across 5 representative participants using all possible channel combinations for channels 1, 2, 3, and 4 for both dry and wet electrodes. Channels positions are $1 \rightarrow O_1$, $2 \rightarrow O_z$, $3 \rightarrow O_2$, $4 \rightarrow PO_z$. Data from table 5.4.
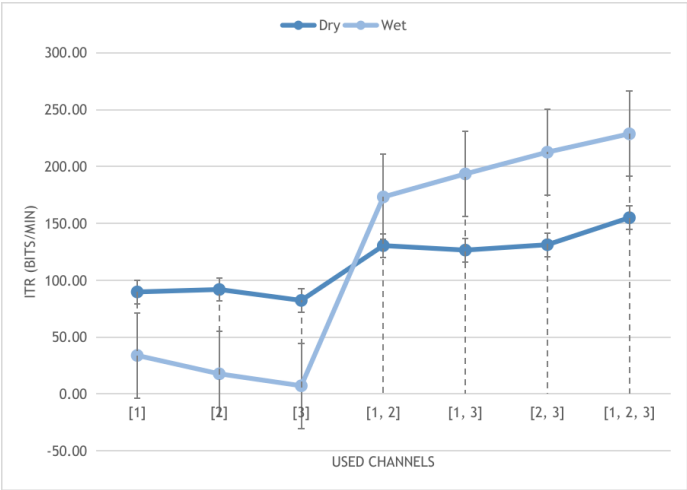
Figure 5.3. Line chart of ITR across 10 participants using all possible channel combinations for channels 1, 2, 3, for both dry and wet electrodes. Channels positions are $1 \rightarrow O_1$, $2 \rightarrow O_z$, $3 \rightarrow O_2$. Data from table 5.3.
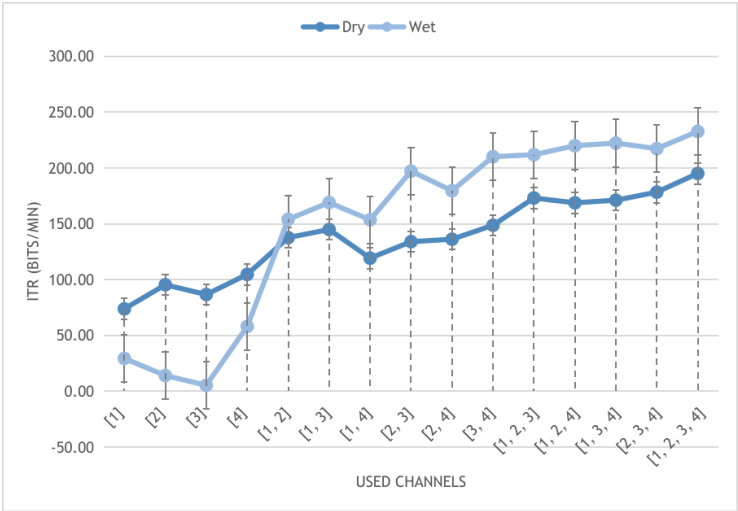
Figure 5.4. Line chart of ITR across 5 representative participants using all possible channel combinations for channels 1, 2, 3, and 4 for both dry and wet electrodes. Channels positions are $1 \rightarrow O_1$, $2 \rightarrow O_z$, $3 \rightarrow O_2$, $4 \rightarrow PO_z$.. Data from table 5.4.

In an effort to see if the number of trainings could be reduced, the following data was obtained. Tables and graphs below show the accuracy and the ITR

of the algorithm, for each participant using 1, 2, 3 or 4 training session.

Trainings / Par. ID	1	2	3	4
1	1.0000	0.9691	0.9857	0.9831
2	0.9487	0.9794	0.9857	0.9888
3	0.7895	0.8229	0.8286	0.8588
4	0.7895	0.7708	0.8129	0.7684
5	0.9474	0.9694	0.9786	0.9719
6	0.9474	0.9474	0.9638	0.9492
7	1.0000	0.9796	0.9859	0.9718
8	0.9474	0.9479	0.9928	0.9718
9	1.0000	1.0000	0.9856	0.9885
10	1.0000	1.0000	0.9929	0.9887
Mean	0.9370	0.9386	0.9512	0.9441
SE	0.0258	0.0246	0.0219	0.0231

Table 5.5. Algorithm accuracy for each one of the participants, based on the number of training sessions for the three wet electrodes.

Figure 5.5. Bar chart of the accuracy of each training session, for the three wet electrodes. Data from table 5.5.

Trainings / Par. ID	1	2	3	4
1	0.6316	0.6354	0.6187	0.6742
2	0.9737	0.9897	0.9929	0.9774
3	0.8947	0.8438	0.8500	0.9096
4	0.7838	0.7579	0.8333	0.7443
5	0.8684	0.8842	0.8188	0.8418
6	0.3947	0.3711	0.4000	0.4157
7	0.8684	0.9063	0.9065	0.9318
8	0.8947	0.9072	0.8440	0.8483
9	0.8974	0.8632	0.8841	0.8362
10	0.8947	0.8737	0.8696	0.8701
Mean	0.8102	0.8032	0.8018	0.8049
SE	0.0545	0.0568	0.0537	0.0514

Table 5.6. Algorithm accuracy for each one of the participants, based on the number of training sessions for the three dry electrodes.

Figure 5.6. Bar chart of the accuracy of each training session, for the three dry electrodes. Data from table 5.6.

Par. ID \ Trainings	1	2	3	4
1	272.41	241.81	256.39	253.98
2	226.14	250.57	256.39	259.35
3	135.90	151.83	154.64	170.35
4	135.90	127.53	146.95	126.45
5	225.16	242.06	249.86	244.15
6	225.16	225.16	237.54	226.46
7	272.41	250.76	256.58	244.02
8	225.16	225.56	263.50	244.02
9	272.41	272.41	256.29	259.09
10	272.41	272.41	263.56	259.29
Mean	226.31	226.01	234.17	228.71
SE	16.62	15.36	14.10	14.15

Table 5.7. ITR for each one of the participants, based on the number of training sessions for the three wet electrodes.
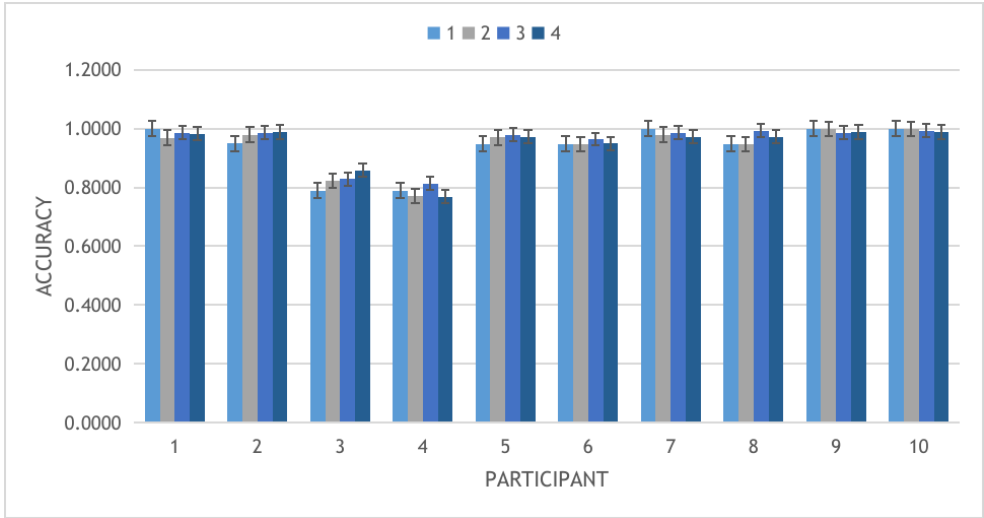

Figure 5.7. Bar chart of the ITR of each training session, for the three wet electrodes. Data from table 5.7.

Par. ID \ Trainings	1	2	3	4
1	74.57	75.83	70.44	89.12
2	245.64	260.27	263.56	248.83
3	190.76	162.39	165.67	199.84
4	133.31	121.92	157.04	116.20
5	175.63	184.57	149.82	161.38
6	16.85	13.22	17.71	20.41
7	175.63	197.75	197.89	214.28
8	190.76	198.35	162.51	164.78
9	192.38	172.74	184.48	158.48
10	190.76	178.57	176.27	176.54
Mean	158.63	156.56	154.54	154.99
SE	21.13	22.12	21.38	20.79

Table 5.8. ITR for each one of the participants, based on the number of training sessions for the three dry electrodes.

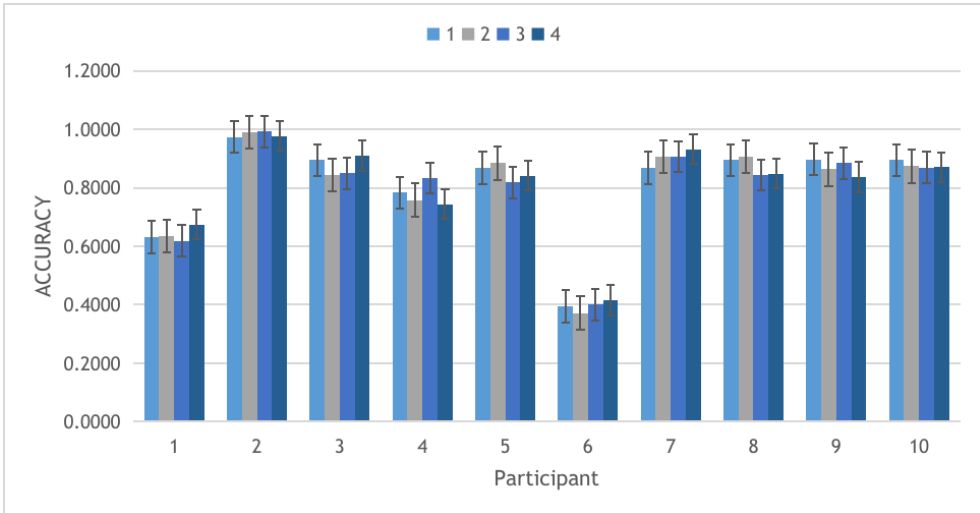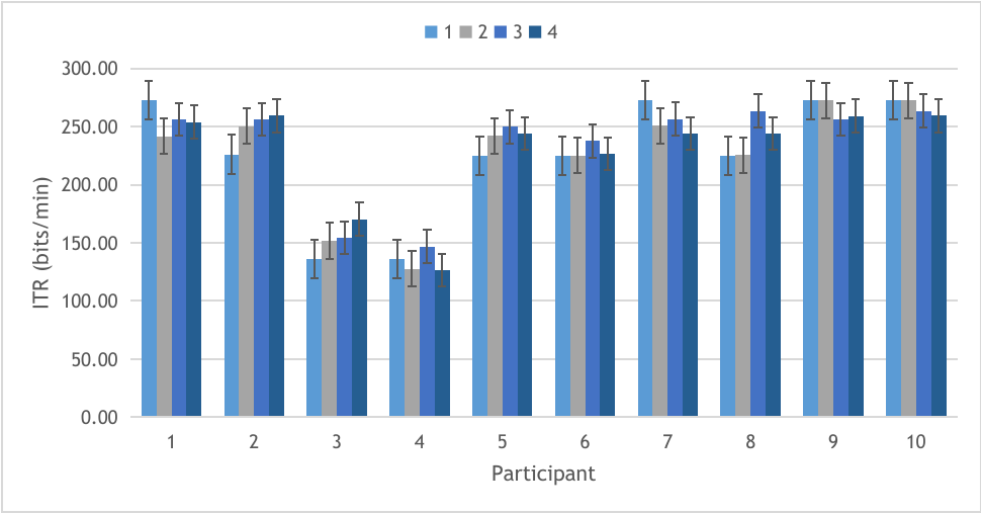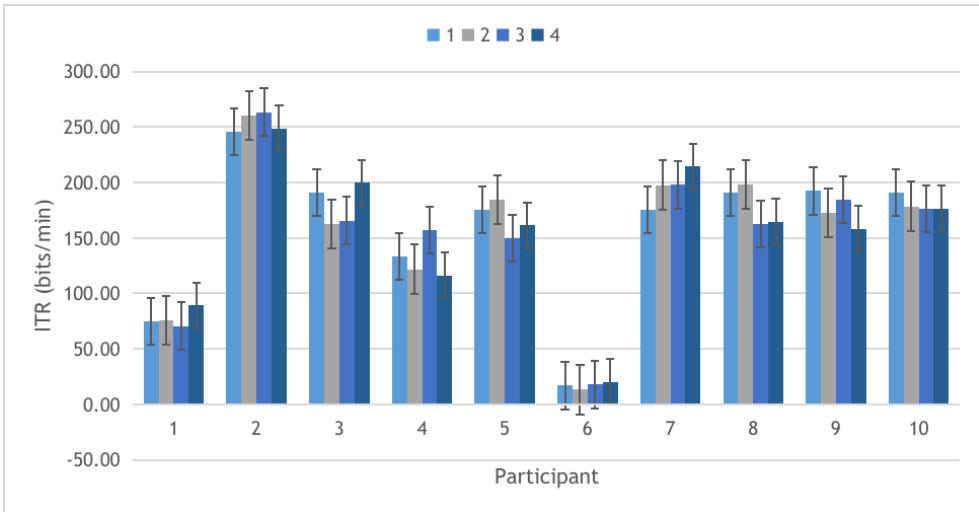**Figure 5.8.** Bar chart of the ITR of each training session, for the three dry electrodes. Data from table 5.8.

For the response time of each one of the system's commands, 5 representative participants were chosen and were asked to use keyboards arrows in

order to check their desired command response time. More specifically, they tried to press the same keyboard arrow as the command they wanted to apply, as simultaneously as possible with the moment, they started focusing on the corresponding target of the visual stimulus interface. The results shown in table 5.9 for dry electrodes and in table 5.10 for the wet.

Participant ID	Forward (sec)	Backward (sec)	Turn right (sec)	Turn left (sec)	Stop (sec)
2	2.27	2.60	3.07	2.19	0.65
4	2.15	0.95	2.67	2.23	1.12
8	2.90	1.53	3.23	2.50	2.15
9	2.22	0.73	2.75	2.31	0.90
10	3.13	3.62	3.11	1.53	2.83
Mean	2.53	1.89	2.97	2.15	1.53
SE	0.16	0.44	0.09	0.13	0.34

Table 5.9. Response time in seconds for each one of the system's commands using dry electrodes. Measured on 5 representative participants.

Participant ID	Forward (sec)	Backward (sec)	Turn right (sec)	Turn left (sec)	Stop (sec)
2	2.19	2.67	2.04	2.00	1.65
4	2.27	1.37	1.62	1.54	0.43
8	2.08	2.83	2.48	2.47	0.90
9	1.60	2.17	1.54	2.77	1.76
10	1.57	1.87	1.63	1.01	1.76
Mean	1.94	2.18	1.86	1.96	1.30
SE	0.12	0.22	0.14	0.26	0.22

Table 5.10. Response time in seconds for each one of the system's commands using wet electrodes. Measured on 5 representative participants.

CHAPTER **6**

Discussion

The results presented in the previous section can lead to important conclusions and observations. It should be noted that half of the participants had never used such a BCI system before, while the participants were not prohibited from moving or talking, during the experiments. Two out of ten participants failed to complete the predefined route due to very low accuracy achieved in the training session. This is most probably related to user's tiredness. Indeed, those participants reported feeling tired and unable to focus well on the targets. Our main conclusions follow next:

- **The use of dry electrodes proves to be feasible.**

  According to tables 5.1 and 5.2, the dry electrodes achieve a high enough accuracy, nearly 80.49%, capable of use in a navigation system. Such a percentage may be sufficient enough to replace the wet electrodes and use dry instead. However, a delay in the predefined route completion time of about 2 minutes was noted. Such a delay is most probably correlated with the lower accuracy of 14.73% of the dry electrodes. Moreover, for dry electrodes, the ITR was reduced to 154.99 $bits/sec$ marking a drop of 32.24%.

- **Dry electrodes seem to be more dependent on the number of used electrodes than their position, while wet electrodes are dependent on both the number of used channels and their position.**

  Graph 5.1 and table 5.3 clearly show that, on one hand, dry electrodes for a single channel system can give a mean value of 64.84% with standard error equal to 0.52%, and for the dual channel system, the accuracy reaches $74.97\% \pm 0.40\%$. On the other hand, for wet electrodes, using one and two channels perform at $38.32\% \pm 4.72\%$ and $87.93\% \pm 2.43\%$, respectively. Using three channels we reach a mean accuracy of equal to $94.41\% \pm 2.31\%$. Those percentages in the standard error show that

when using dry electrodes, one should pay closer attention to the total
number of the channels used than their exact positioning, since they
will most probably perform equally good. However, regarding the wet
electrodes, the user should pay attention to both the total number of
channels used and their positions. Findings are reflected in graph 5.2
and table 5.4.

- **We can achieve reliable navigation with two or three channels.**

  According to table 5.3, the use of a single wet electrode can achieve a
  mean accuracy of 38.32%, while dry electrodes achieve a mean accuracy
  of 64.84%, values not acceptable for an easy-controlling navigation sys-
  tem. The use of two different wet electrodes can give accuracies ranging
  from 83.63% to 92.03%, and ITRs from 126.51 bits/sec to 131.24 bits/sec.
  As far as dry electrodes are concerned, dual channel and triple channel
  setup provide accuracies of 74.97% and 80.49%, respectively. Despite
  the fact that dry electrodes do have better single-channel results com-
  pared to the wet ones, they have worse performance contrary to single
  channel accuracy, presented on the study of Farmaki et al. [1] (81.00%).
  In order though to achieve accuracies close to 81.00%, we need to use,
  dual channel setup in the case of wet electrodes and triple channels setup
  in the case of the dry ones.

  It is worth noting that one of the participants managed to have an
  accuracy of 98.8% with only one channel, using a dry electrode placed
  in PO_z, which makes the system possibly usable with minimum setup of
  only one dry electrode. The same participant using three channels had
  an accuracy of 87.01%, while the addition of a fourth channel, increased
  accuracy to 98.31%.

- **The system's performance is not fully dependent on accuracy.**

  It should be noted that the completion time of the route was not com-
  pletely dependent on the accuracy of the system, as several of the partic-
  ipants who achieved low accuracy managed to complete the route faster
  than others with a higher one. A noteworthy example is subject 4, who
  managed to finish the predefined route in the best time of 3:23.19 min-
  utes, having the worst accuracy (76.84%) across all 10 participants, as
  shown in table 5.1. Some significant factors to take into account are the
  familiarization with the system and the ability to anticipate the response
  time of each command in order to compensate for this latency.

- **The number of training sessions could be reduced without compromising the system's efficiency.**

  Paying attention to tables 5.5, 5.6, 5.7, 5.8 and their corresponding bar charts, we can observe that less than four training sessions could be used in our system. More specifically, according to the specific tables, the ideal scenario was to use only three sessions for either dry or wet electrodes. We reached this conclusion because, according to tables 5.5 and 5.6, the addition of the fourth session does not seem to increase the system's effectiveness, which may be due to the fact that participants experience fatigue. More specifically, with four training sessions, wet electrodes accuracy and ITR, was reduced by 0.75% and 2.33%, respectively, while dry electrodes show improvement of 0.39% and 0.29% for the same metrics, respectively. Even though one or two training sessions in the current set-up achieve high accuracies and ITRs, we do not consider this a reliable result, since the data samples used for the training of the classifier are very few. Consequently, the use of three sessions seems like the most appropriate choice, since most of the participants reported that four training sessions were quite tiring.

- **The number of targets could be reduced without deteriorating system's mobility degrees of freedom.**

  From Tables 5.9 and 5.10, we can see that across three out four commands, the maximum difference we encounter in response time, using dry instead of wet electrodes, is equal to $0.6s$. The minimum difference presented across those commands was captured on the "left" turn, which was equal to $0.19s$. However, the maximum difference of all four commands captured in the "right" turn command, which is equal to $1.11s$. Keeping this in mind, we could use the three targets-frequencies that presented the higher SNR, for the three commands -forward, right, left- and reduce the average response time for the whole system from $2.21s$ to $2.03s$ for the dry electrodes and from $1.85s$ to $1.77s$ for the wet ones, 8.5% and 4.51% reduction respectively. Moreover, all participants stated that they did not need the backward command since the robot used in the experiment and most electric wheelchairs generally have the ability to rotate around themselves. This would also reduce the training time, which in combination with fewer training sessions has the potential to lead to a much convenient and easy-to-use system.

Taking everything into account, the OpenBCI Cyton board can be suc-
cessfully used for such a navigation system with acceptable values of accuracy
and ITR, which vary depending on the number of the channels used and their
placement. However, we could not attain reliable navigation using a single
channel, as opposed to using a costly commercial EEG recorder, which was
the case in [1]. Comparing the system's response reported in [1] with the cur-
rent one, according to tables 5.9 and 5.10, we observe that the response time
across all possible commands for our system lies at $2.21s$ for dry and $1.85s$ for
the wet ones, 25.77% and 5.05% higher than the referred study (reported to be
$1.76s$ for one wet electrode), but not high enough to be a factor for rejecting
our system contrary to a commercial EEG recording device. Considering the
Cyton board's cost, the acceptable value of accuracy and the high value of
ITR, it is a satisfactory choice for building a cost-effective SSVEP-based BCI
system.

CHAPTER 7

Conclusion and future work

In the present study, a low cost SSVEP based BCI system for navigation purposes was developed. The results showed that the system is fully functional for wet electrodes. The system was also functional for eight out of ten participants using the dry electrodes, achieving a lower accuracy compared to wet ones. In the future we plan to reduce the number of visual stimuli to three, by choosing the three optimal frequencies for each subject. In addition, all participants stated that they did not need the backward command, since the robot used in the experiment and most electric wheelchairs generally have the ability to rotate around themselves. Finally, we plan to explore various channel selection algorithms, in order to reduce the number of channels used and thus simplify the preparation of the system before use. In this way, the user will be able to benefit from the system by collecting data from only one channel as mentioned above.

Bibliography

[1] C. Farmaki, M. Krana, M. Pediaditis, E. Spanakis, and V. Sakkalis, "Single-channel ssvep-based bci for robotic car navigation in real world conditions," in *2019 IEEE 19th International Conference on Bioinformatics and Bioengineering (BIBE)*, pp. 638–643, 2019.

[2] "Brain Anatomy and How the Brain Works." https://www.hopkinsmedicine.org/health/conditions-and-diseases/anatomy-of-the-brain.

[3] "Anatomy of the Brain." https://mayfieldclinic.com/pe-anatbrain.htm.

[4] M. Matthew Hoffman, "Picture of the Brain." https://www.webmd.com/brain/picture-of-the-brain.

[5] M. Teplan, "Fundamental of eeg measurement," *MEASUREMENT SCIENCE REVIEW*, vol. 2, 01 2002.

[6] S. N. Abdulkader, A. Atia, and M.-S. M. Mostafa, "Brain computer interfacing: Applications and challenges," *Egyptian Informatics Journal*, 2015.

[7] R. Upadhyay, P. K. Kankar, P. K. Padhy, and V. K. Gupta, "Extraction and classification of electroencephalogram signals," in *2012 IEEE International Conference on Computational Intelligence and Computing Research*, pp. 1–4, 2012.

[8] P. A. Abhang, B. W. Gawali, and S. C. Mehrotra, "Chapter 2 - technological basics of eeg recording and operation of apparatus," in *Introduction to EEG- and Speech-Based Emotion Recognition* (P. A. Abhang, B. W. Gawali, and S. C. Mehrotra, eds.), pp. 19–50, Academic Press, 2016.

[9] J. D. Lewine and W. W. Orrison, "Chapter 8 - clinical electroencephalography and event-related potentials," in *Functional Brain Imaging* (W. W. Orrison, J. D. Lewine, J. A. Sanders, and M. F. Hartshorne, eds.), pp. 327–368, Mosby, 1995.

[10] N. Kulkarni and V. Bairagi, "Chapter two - electroencephalogram and its use in clinical neuroscience," in *EEG-Based Diagnosis of Alzheimer Disease* (N. Kulkarni and V. Bairagi, eds.), pp. 25–35, Academic Press, 2018.

[11] Q. Ai, Q. Liu, W. Meng, and S. Q. Xie, "Chapter 2 - state-of-the-art," in *Advanced Rehabilitative Technology* (Q. Ai, Q. Liu, W. Meng, and S. Q. Xie, eds.), pp. 11–32, Academic Press, 2018.

[12] M. Sazgar and M. G. Young, *EEG Artifacts*, pp. 149–162. Cham: Springer International Publishing, 2019.

[13] J. Knight, "Signal fraction analysis and artifact removal in eeg," 12 2008.

[14] M. K. Islam, A. Rastegarnia, and Z. Yang, "Methods for artifact detection and removal from scalp eeg: A review," *Neurophysiologie Clinique/Clinical Neurophysiology*, vol. 46, no. 4, pp. 287–305, 2016.

[15] J. A. Urigüen and B. Garcia-Zapirain, "EEG artifact removal—state-of-the-art and guidelines," *Journal of Neural Engineering*, vol. 12, p. 031001, apr 2015.

[16] T. B. Team, "All about EEG artifacts and filtering tools." https://www.bitbrain.com/blog/eeg-artifacts, 2020.

[17] J. D. Kropotov, "Chapter 1.6 - event-related potentials," in *Functional Neuromarkers for Psychiatry* (J. D. Kropotov, ed.), pp. 59–78, San Diego: Academic Press, 2016.

[18] A. M. Norcia, L. G. Appelbaum, J. M. Ales, B. R. Cottereau, and B. Rossion, "The steady-state visual evoked potential in vision research: A review," *Journal of Vision*, vol. 15, pp. 4–4, 05 2015.

[19] S. K. Mudgal, S. K. Sharma, J. Chaturvedi, and A. Sharma, "Brain computer interface advancement in neurosciences: Applications and issues," *Interdisciplinary Neurosurgery*, vol. 20, p. 100694, 2020.

[20] Y. M. Chi, Y.-T. Wang, Y. Wang, C. Maier, T.-P. Jung, and G. Cauwen-
     berghs, "Dry and noncontact eeg sensors for mobile brain–computer in-
     terfaces," *IEEE Transactions on Neural Systems and Rehabilitation En-
     gineering*, vol. 20, no. 2, pp. 228–235, 2012.

[21] C. Guger, G. Krausz, and G. Edlinger, "Brain-computer interface control
     with dry eeg electrodes," 01 2011.

[22] M. A. Lopez-Gordo, D. Sanchez-Morillo, and F. P. Valle, "Dry eeg elec-
     trodes," *Sensors*, vol. 14, no. 7, pp. 12847–12870, 2014.

[23] P. Fiedler, J. Haueisen, D. Jannek, S. Griebel, L. Zentner, F. Vaz, and
     C. Fonseca, "Comparison of three types of dry electrodes for electroen-
     cephalography," *ACTA IMEKO*, vol. 3, pp. 33–37, 09 2014.

[24] G. Rojas, C. Alvarez, C. Montoya Moya, M. de la Iglesia Vaya, J. Cister-
     nas, and M. Gálvez, "Study of resting-state functional connectivity net-
     works using eeg electrodes position as seed," *Frontiers in Neuroscience*,
     vol. 12, 03 2018.

[25] G. H. Klem, H. Lüders, H. H. Jasper, and C. E. Elger, "The ten-twenty
     electrode system of the international federation. the international feder-
     ation of clinical neurophysiology.," *Electroencephalography and clinical
     neurophysiology. Supplement*, vol. 52, 1999.

[26] G. M. Rojas, C. Alvarez, C. E. Montoya, M. de la Iglesia-Vayá, J. Cister-
     nas, and M. Gálvez, "Study of resting-state functional connectivity net-
     works using eeg electrodes position as seed," *Frontiers in Neuroscience*,
     vol. 12, 2018.

[27] B. He, B. Baxter, B. J. Edelman, C. C. Cline, and W. W. Ye, "Noninva-
     sive brain-computer interfaces based on sensorimotor rhythms," *Proceed-
     ings of the IEEE*, vol. 103, no. 6, pp. 907–925, 2015.

[28] Y.-P. Lin, Y. Wang, and T.-P. Jung, "A mobile ssvep-based brain-
     computer interface for freely moving humans: The robustness of canoni-
     cal correlation analysis to motion artifacts," in *2013 35th Annual Inter-
     national Conference of the IEEE Engineering in Medicine and Biology
     Society (EMBC)*, pp. 1350–1353, 2013.

[29] L. Angrisani, P. Arpaia, D. Casinelli, and N. Moccaldi, "A single-channel
     ssvep-based instrument with off-the-shelf components for trainingless

brain-computer interfaces," *IEEE Transactions on Instrumentation and Measurement*, vol. 68, no. 10, pp. 3616–3625, 2019.

[30] Y.-T. Wang, Y. Wang, and T.-P. Jung, "A cell-phone-based brain–computer interface for communication in daily life," *Journal of Neural Engineering*, vol. 8, p. 025018, mar 2011.

[31] Y.-P. Lin, Y. Wang, C.-S. Wei, and T.-P. Jung, "A mobile brain-computer interface for freely moving humans," pp. 448–453, 07 2013.

[32] K. Mohanchandra and S. Saha, "A communication paradigm using subvocalized speech: Translating brain signals into speech," *Augmented Human Research*, vol. 1, 10 2016.

[33] R. Djemal, A. Bazyed, K. Belwafi, S. Gannouni, and W. Kaaniche, "Three-class eeg-based motor imagery classification using phase-space reconstruction technique," *Brain sciences*, vol. 6, 08 2016.

[34] P. Xanthopoulos, P. M. Pardalos, and T. B. Trafalis, *Linear Discriminant Analysis*, pp. 27–33. New York, NY: Springer New York, 2013.

[35] "PsychoPy." https://www.psychopy.org/.

[36] "OpenBCI Cyton board." https://docs.openbci.com/Cyton/CytonLanding/.

[37] "Nexus robot." https://www.nexusrobot.com/product/4wd-mecanum-wheel-mobile-arduino-robotics-car-10011.html.